10 E. Oberlin, A. Amara, F. Bachelerie, C. Bessia, J. L. Virelizier, F. Arenzana-Seisdedos, O. Schwartz, J. M. Heard, I. Clark-Lewis, D. L. Legler, M. Loetscher, M. Baggiolini and B. Moser, *Nature*, 1996, **382**, 833–835.
11 Y. Feng, C. C. Broder, P. E. Kennedy and E. A. Berger, *Science*, 1996, **272**, 872–877.
12 A. Müller, B. Homey, H. Soto, N. Ge, D. Catron, M. E. Buchanan, T. Mcclanahan, E. Murphy, W. Yuan, S. M. Wagner, J. L. Barrera, A. Mohar, E. Vera'stegui and A. Zlotnik, *Nature*, 2001, **410**, 50–56.
13 J. A. Burger, M. Burger and T. J. Kipps, *Blood*, 1999, **94**, 3658–3667.
14 T. Nanki, K. Hayashida, H. S. EI-Gabalawy, S. Suson, K. Shi, H. J. Girschick, S. Yavuz and P. E. Lipsky, *J. Immunol.*, 2000, **165**, 6590–6598.
15 T. Murakami, T. Nakajima, Y. Koyanagi, K. Tachibana, N Fujii, H. Tamamura, N. Toshida, M. Waki, A. Matsumoto, O. Yoshie, T. Kishimoto, N. Yamamoto and T. Nagasawa, *J. Exp. Med.*, 1997, **186**, 1389–1393.
16 H. Tamamura, A. Hori, N. Kanzaki, K. Hiramatsu, M. Mizumoto, H. Nakashima, N. Yamamoto, A. Otaka and N. Fujii, *FEBS Lett.*, 2003, **550**, 79–83.
17 H. Tamamura, M. Fujisawa, K. Hiramatsu, M. Mizumoto, H. Nakashima, N. Yamamoto, A. Otaka and N Fujii, *FEBS Lett.*, 2004, **569**, 99–104.
18 D. Schols, S. Struyf, J. Van Damme, J. A. Este, G. Henson and E. DeClarcq, *J. Exp. Med.*, 1997, **186**, 1383–1388.
19 G. A. Donzella, D. Schols, S. W. Lin, J. A. Este and K. A. Nagashima, *Nat. Med.*, 1998, **4**, 72–76.
20 K. Ichiya, S. Yokoyama-Kumakura, Y. Tanaka, R. Tanaka, K. Hirose, K. Bannai, T. Edamatsu, M. Yanaka, Y. Niitani, N. Miyano-Kurosaki, H. Takaku, Y. Koyanagi and N. Yamamoto, *Proc. Natl. Acad. Sci. U. S. A.*, 2003, **100**, 4185–4190.
21 M. Masuda, H. Nakashima, T. Ueda, H. Naba, R. Ikoma, A. Otaka, Y. Terakawa, H. Tamamura, T. Ibuka, T. Murakami, Y. Koyanagi, M. Waki, A. Matsumoto, N. Yamamoto and N. Fujii, *Biochem. Biophys. Res. Commun.*, 1992, **189**, 845–850.
22 Tamamura, Y Xu, T. Hattori, X. Zhang, R. Arakaki, K. Kanbara, A. Omagari, A. Otaka, T. Ibuka, N. Yamamoto, H. Nakashima and N. Fujii, *Biochem. Biophys. Res. Commun.*, 1998, **253**, 877–882.
23 N. Fujii, S. Oishi, K. Hiramatsu, T. Araki, S. Ueda, H. Tamamura, A. Otaka, S. Kusano, S. Terakubo, H. Nakashima, J. A. Broach, J. O. Trent, Z. Wang and S. C. Peiper, *Angew. Chem., Int. Ed.*, 2003, **42**, 3251–3253.
24 H. Tamamura, K. Hiramatsu, M. Mizumoto, S. Ueda, S. Kusano, S. Terakubo, M. Akamatsu, N. Yamamoto, J. O. Trent, Z. Wang, S. C. Peiper, H. Nakashima, A. Otaka and N. Fujii, *Org. Biomol. Chem.*, 2003, **1**, 3663–3669.
25 H. Tamamura, T. Araki, S. Ueda, Z. Wang, S. Oishi, A. Esaka, J. O. Trent, H. Nakashima, N. Yamamoto, S. C. Peiper, A. Otaka and N. Fujii, *J. Med. Chem.*, 2005, **48**, 3280–3289.
26 H. Tamamura, A. Esaka, T. Ogawa, T. Araki, S. Ueda, Z. Wang, J. O. Trent, H. Tsutsumi, H. Masuno, H. Nakashima, N. Yamamoto, S. C. Peiper, A. Otaka and N. Fujii, *Org. Biomol. Chem.*, 2005, **3**, 4392–4394.
27 S. Ueda, S. Oishi, Z. Wang, T. Araki, H. Tamamura, J. Cluzeau, H. Ohno, S. Kusano, H. Nakashima, J. O. Trent, S. C. Peiper and N. Fujii, *J. Med. Chem.*, 2007, **50**, 192–198.
28 W. Zhan, Z. Liang, A. Zhu, S. Kurtkaya, H. Shim, J. P. Snyder and D. C. Liotta, *J. Med. Chem.*, 2007, **50**, 5655–5664.
29 T. Tanaka, H. Tsutsumi, W. Nomura, Y. Tanabe, N. Ohashi, A. Esaka, C. Ochiai, J. Sato, K. Itotani, T. Murakami, K. Ohba, N. Yamamoto, N. Fujii and H. Tamamura, *Org. Biomol. Chem.*, 2008, **6**, 4374–4377.
30 H. Tamamura, K. Hiramatsu, S. Kusano, S. Terakubo, N. Yamamoto, J. O. Trent, Z. Wang, S. C. Peiper, H. Nakashima, A. Otaka and N. Fujii, *Org. Biomol. Chem.*, 2003, **1**, 3656–3662.
31 J. M. Navenot, Z. X. Wang, J. O. Trent, J. L. Murray, Q. X. Hu, L. DeLeeuw, P. S. Moore, Y. Chang and S. C. Peiper, *J. Mol. Biol.*, 2001, **59**, 380–393.

Research Article

Journal of Peptide

Received: 4 April 2009 Revised: 11 June 2009 Accepted: 15 June 2009 Published online in Wiley Interscience: 11 August 2009

(www.interscience.com) DOI 10.1002/psc.1161

Synthesis of protein kinase Cδ C1b domain by native chemical ligation methodology and characterization of its folding and ligand binding‡

Nami Ohashi,[a] Wataru Nomura,[a]* Mai Kato,[a] Tetsuo Narumi,[a] Nancy E. Lewin,[b] Peter M. Blumberg[b] and Hirokazu Tamamura[a]*

The C1b domain of protein kinase Cδ (PKCδ), a potent receptor for ligands such as diacylglycerol and phorbol esters, was synthesized by utilizing native chemical ligation. With this synthetic strategy, the domain was efficiently constructed and shown to have high affinity ligand binding and correct folding. The C1b domain has been utilized for the development of novel ligands for the control of phosphorylation by PKC family members. This strategy will pave the way for the efficient construction of C1b domains modified with fluorescent dyes, biotin, etc. Copyright © 2009 European Peptide Society and John Wiley & Sons, Ltd.

Supporting information may be found in the online version of this article

Keywords: protein kinase C; native chemical ligation; C1b domain; ligand binding

Introduction

Protein kinase C (PKC) isoforms are serine/threonine protein kinases which play a pivotal role in physiological responses to growth factors, oxidative stress, and tumor promoters. These responses regulate numerous cellular processes [1,2], including proliferation [3], differentiation [4], migration [5], and apoptosis [6,7]. Under physiological conditions, signal transduction through PKC is triggered by the interaction between diacylglycerol (DAG), a lipid second messenger, and the C1 domains of PKC. The C1 domain is well conserved within the PKC superfamily, forming a zinc finger structure into which the DAG or phorbol ester inserts. Ten PKC isoforms have been described, among which PKCδ, a member of the novel PKC subfamily, is DAG/phorbol ester-dependent but calcium-insensitive. Development of ligands with high specificity for PKC isozymes has been a critical issue [8–10]. Considerable attention has been directed at the development of inhibitors of PKC isoforms; however, for PKCδ, activators have a therapeutic rationale. For example, PKCδ is growth-inhibitory in NIH3T3 cells, whereas PKCα and PKCε are growth-stimulatory [10]. Thus, complementary therapeutic strategies are to inhibit a specific PKC isoform or to stimulate an antagonistic isoform. For this latter approach, activators selective for different isoforms are needed.

For the development of isozyme-specific ligands, the C1b domain provides a robust platform for binding analyses. Although bacterial expression of cloned C1b domain affords ample material, preparation of the C1b domain by synthetic methods would greatly enhance its ability to be manipulated, such as by labeling with fluorescent dyes or biotin. However, synthesis of the C1b domain by standard SPPS is problematic on account of its size (~50 amino acids), although its synthesis by a stepwise condensation method has proven possible [11]. In this study, we applied native chemical ligation (NCL) methodology [12,13] to an efficient synthesis of the PKCδ C1b (δC1b) domain (Scheme 1).

Materials and Methods

Preparation of amino acid-loaded 2-chlorotrityl resin

2-Chlorotrityl chloride resin (100–200 mesh polystyrene, 1% DVB, 1.4 meq/g, 1.4 mmol) (Novabiochem) was treated with Fmoc-His(Trt)-OH (0.63 mmol) and *N,N*-diisopropylethylamine (DIPEA) (2.25 mmol) in dry DCM (10 ml) for 1 h. The resin was dried *in vacuo* after washing with dry DCM. The loading was determined by measuring UV absorption at 301 nm of the piperidine-treated Fmoc-His(Trt)-(2-Cl)Trt-resin (0.32 meq/g). Unreacted chloride was capped by treatment with MeOH (1 ml), DCM (10 ml), and DIPEA (574 μl, 3.3 mmol) for 15 min.

Synthesis of peptide thioester δC1b(231–246)

The peptide chain was manually constructed using Fmoc-based solid-phase synthesis on Fmoc-His(Trt)-(2-Cl)Trt-resin with capping

* *Correspondence to: Wataru Nomura and Hirokazu Tamamura, Institute of Biomaterials and Bioengineering, Tokyo Medical and Dental University, 2-3-10 Kandasurugadai, Chiyoda-ku, Tokyo 101-0062, Japan. E-mail: tamamura.mr@tmd.ac.jp; nomura.mr@tmd.ac.jp*

a *Institute of Biomaterials and Bioengineering, Tokyo Medical and Dental University, 2-3-10 Kandasurugadai, Chiyoda-ku, Tokyo 101-0062, Japan*

b *Laboratory of Cancer Biology and Genetics, Center for Cancer Research, National Cancer Institute, National Institutes of Health, Bethesda, MA 20892, USA*

‡ *Dedicated to Dr. Victor E. Marquez on the occasion of his 65th birthday.*

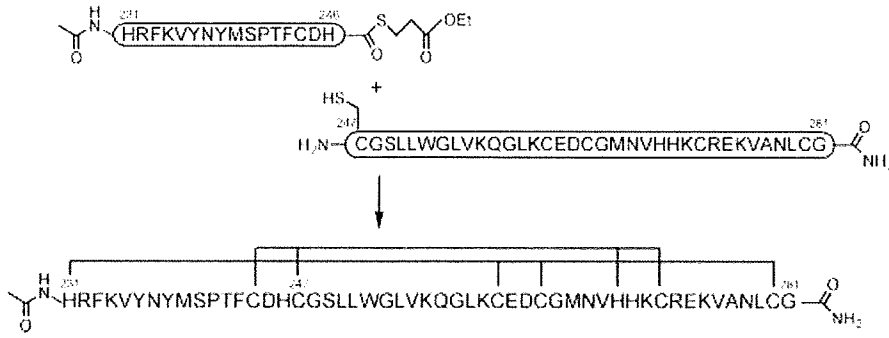

Scheme 1. Process of NCL methodology and the sequence of synthesized δ C1b domain. The amino acid residues involved in chelation of zinc ions are grouped by lines.

(0.05 mmol scale). Fmoc-protected amino acid derivatives (5 equiv) were successively condensed using 1,3-diisopropylcarbodiimide (DIPCI) (5 equiv) in the presence of HOBt·H_2O (5 equiv) in DMF (2 ml) (90 min treatment). The following side-chain protecting groups were used: Boc for Lys, Pbf for Arg, OBu^t for Asp, Trt for Asn, Cys, and His, Bu^t for Ser, Thr, and Tyr. The Fmoc group was deprotected with 20% piperidine in DMF (2 ml) for 15 min. After the final Fmoc deprotection, the peptide was acetylated in the mixture of Ac_2O–DMF–pyridine (1 : 4 : 1, v/v, 3 ml). The yield of the resulting protected peptide resin was 335 mg. The resulting protected δC1b(231–246) was cleaved from the resin with TFE–AcOH–DCM (1 : 1 : 3, v/v, 15 ml) (2 h treatment), and thioesterified with ethyl mercaptopropionate (20 equiv), HOBt·H_2O (10 equiv), and 1-(3-dimethylaminopropyl)-3-ethylcarboiimide (EDCI)·HCl (10 equiv) in DMF (1 ml) (0 C, 2 h). Subsequently, the peptide was deprotected with TFA–thioanisole–*m*-cresol–triisopropylsilane (TIS) (89 : 7.5 : 2.5 : 1, v/v, 5 ml) (90 min treatment). After cleavage and deprotection, the crude product was precipitated and washed three times with cold diethyl ether, then purified by RP-HPLC (column: COSMOSIL $_5C_{18}$ AR-II, 10 × 250 mm).

Synthesis of peptide fragment δC1b(247–281)

The peptide chain was manually constructed using Fmoc-based solid-phase synthesis on NovaSyn TGR-resin (0.26 meq/g, 0.1 mmol scale). Fmoc-protected amino acid derivatives (5 equiv) were successively condensed using DIPCI (5 equiv) in the presence of HOBt·H_2O (5 equiv) in DMF (4 ml) (90 min treatment). The side-chain protecting groups were used as for the synthesis of δC1b(231–246). Additionally, Trt and OBu^t were used for Gln and Glu, respectively. The yield of the resulting protected peptide resin was 920 mg. Protected δC1b(247–281) was cleavaged and deprotected with TFA–thioanisole–*m*-cresol–TIS (89 : 7.5 : 2.5 : 1, v/v, 10 ml) (90 min treatment). The purification procedure was the same as in the synthesis of δC1b(231–246).

Native chemical ligation

The thioester peptide (δC1b(231–246): 2.9 mg, 1.3 μmol), the *N*-terminal Cys peptide (δC1b(247–281): 4.9 mg, 1.3 μmol), and tris(2-carboxyethyl)phosphine hydrochloride (3 mg, 13 μmol) were dissolved in 1.5 ml of 6 M guanidine hydrochloride, 2 mM EDTA, and 0.1 M sodium phosphate at pH 8.5. The addition of 4% thiophenol promoted the conversion of the less reactive 2-mercaptopropionate thioester to the more reactive phenyl-α-thioester and started the ligation reaction [13,14]. After incubation at 37 °C under N_2 atmosphere, the reaction mixture was analyzed by analytical RP-HPLC (column: COSMOSIL $_5C_{18}$ AR-II, 4.6 × 250 mm, a linear gradient of 25–45% acetonitrile, 30 min). The eluent was monitored at 220 nm and characterized by ESI-MS. The product was gel filtrated with Sephadex G-10 and purified by RP-HPLC under the same condition as for peptide fragments.

ESI-MS sample preparation of the folded domain with zinc ion

The synthetic δC1b domain in ultra pure water was treated with 3 molar equivalents of $ZnCl_2$. After incubation at 4 °C for 10 min, the solution was neutralized with 10 mM of pyridinium acetate buffer (pH 6.8). The peptide concentration was adjusted to 50 μM.

Expression and purification of recombinant δC1b domain

The recombinant δC1b domain was expressed as a GST fusion domain. The protein was purified by GSTrap (GE Healthcare) following the manufacturer instruction, then the GST domain was cleaved by treatment with thrombin at 4 C for 12 h. The δC1b domain was further purified by size-exclusion chromatography. The purity of the domain was confirmed as >90% by SDS-PAGE [17].

CD spectroscopy

UV CD spectra were recorded on a Jasco J-720 spectropolarimeter at 25 C. The measurements were performed using a 0.1 cm path length cuvette at a 0.1 nm spectral resolution. Each spectrum represents the average of ten scans, and the scan rate was 50 nm/min. The initial measurement solution contained 50 μM peptide, 50 mM Tris-HCl (pH 7.5), and 1 mM DTT. $ZnCl_2$ was added to the mixture at 100 μM. To measure the unfolded state of synthetic δC1b domain, EDTA was added to the folded peptide mixture at 100 μM.

[^{3}H]-phorbol 12, 13-dibutylate binding

[^{3}H]-phorbol 12, 13-dibutyrate (PDBu) binding to PKC was measured by the polyethylene glycol precipitation assay as described in Refs. 15,16 with minor modification. To determine the dissociation constant (K_d) for the synthetic δC1b, saturation curves with increasing concentrations of the [^{3}H]PDBu were obtained in triplicate. The 250 μl of assay mixture contained 50 mM Tris-HCl (pH 7.4), 1 mM ethyleneglycol-*bis*(β-aminoethyl)-*N,N,N',N'* tetraacetic acid (EGTA), 0.1 mg/ml phosphatidylserine,

2 mg/ml bovine immunoglobulin G, variable concentrations of [^{3}H]PDBu and nonspecific line containing the excessive amount of nonradioactive PDBu against [^{3}H]PDBu. After the addition of peptides stored in 0.015% Triton X-100, binding was carried out at 18 °C for 10 min. Samples were incubated on ice for 10 min. To precipitate peptides, 200 µl of 35% polyethylene glycol in 50 mM Tris-HCl (pH 7.4) was added, then vortexed, and the samples were further incubated on ice for 10 min. The tubes were centrifuged at 4 °C (12,200 rpm, 15 min), then 100 µl aliquot of each supernatant was transferred to scintillation vials for the determination of free [^{3}H]PDBu. Remaining supernatant was aspirated off, and the bottom of centrifuge tube was cut off just above the pellet and transferred to a scintillation vial for the determination of total bound [^{3}H]PDBu.

Results and Discussion

In the synthesis of the δC1b domain, the *N*-terminal (δC1b(231–246)) and *C*-terminal (δC1b(247–281)) peptide fragments were synthesized separately. In this case, an unprotected peptide δC1b(231–246) α-carboxythioester was reacted with another peptide containing an *N*-terminal cysteine residue, δC1b(247–281) [17]. The δC1b(231–246) and δC1b(247–281) fragment peptides were synthesized by Fmoc-based SPPS on a 2-chlorotrityl resin and on a Rink amide resin (NovaSyn TGR), respectively, as described in Materials and Methods Section. The fragment peptides were purified by RP HPLC and characterized by electrospray ionization time-of-flight mass spectrometry (ESI-TOFMS) using a DALTONICS (BRUKER): δC1b(231–246) α-carboxythioester *m/z* [M+H$^+$] calcd: 2203.5, observed: 2203.8; δC1b(247–281) *m/z* [M+H$^+$] calcd: 3829.6, observed: 3829.3. The purification by HPLC (column: COSMOSIL 5C18 AR-II, 20 × 250 mm, a linear gradient of 25–30% acetonitrile in water for δC1b(231–246) α-carboxythioester and a 29% acetonitrile isocratic elution for δC1b(247–281), 30 min) gave pure fragment peptides δC1b(231–246) α-carboxythioester and δC1b(247–281) in overall yields of 35% and 8%, respectively. The purified peptides were lyophilized and dissolved in buffer before the ligation reaction. Charts (A–C) in Figure 1 show the progress of the ligation reaction at 0, 6.5 and 18 h incubation, respectively. The labeled peak c shows thiophenol. The other peaks were identified by ESI-MS; a, δC1b(231–246) (2-mercaptopropionate thioester); b, δC1b(247–281); d, δC1b(231–281) *m/z* [M+H$^+$] calcd: 5898.8, observed: 5899.0. Purification by RP HPLC (column: COSMOSIL 5C18 AR-II, 10 × 250 mm, a linear gradient of 30–45% acetonitrile, 30 min) gave pure δC1b(231–281) in 45% overall yield. Although the δC1b domain contains six cysteine residues, the synthesis of this peptide was efficiently achieved using the ligation technique. Formerly, Futaki *et al.* [18] performed the synthesis of a Cys_2His_2-type zinc finger peptide by applying the NCL method. They showed that this method could apply to the synthesis of more than 90 amino acid peptide and that the synthetic peptide shows correct domain folding and zinc ion chelating as a recombinant protein. In their synthesis, the ligation junction was between methionine and cysteine at the linker residues of the zinc finger peptide. For the δC1b domain, we first attempted ligation at Phe243 and Cys244 junction because of slight possibility of epimerization in thioesterification. After confirmation of low reactivity at this junction, His246 and Cys247 junction was adopted as NCL junction. His–Cys junction has been indicated as very fast kinetics (less than 4 h to complete ligation, when compared to Phe–Cys junction which showed approximately 20% reaction after 48 h) residues for NCL reaction. [19]. However, the thioesterification at the *C*-terminal histidine residue could cause epimerization. To avoid epimerization, the reaction was performed under acidic conditions and low temperature (~0 C) [17]. After NCL reaction, the epimerization of δC1b domain was investigated by isocratic HPLC. To identify the isomer of δC1b domain, D-His incorporated fragment of δC1b(231–246) was synthesized and utilized for NCL. The retention time of D-His δC1b(231–281) was compared with those of L-His domains ligated under −20 and 0 °C. The eluent peaks were identified by ESI-MS. The results indicate that the synthetic δC1b(231–281) contains undetectable level of the isomer form (see Figure S1, Supporting Information).

Folding properties of the peptide were assessed by CD spectra [11]. X-ray crystallography analysis of the δC1b domain has revealed that the domain is a cysteine-rich zinc finger structure with two zinc ions as cofactors [20]. Upon the addition of 2 molar equivalents of zinc ion to the peptide solution, a red-shift at the absorption minimum of the spectrum was observed (Figure 2). The spectrum for the folded δC1b domain was similar to that of the native δC1b domain obtained as a recombinant protein domain. The recombinant δC1b domain was expressed in *Escherichia coli* and purified by GST-affinity chromatography. On the basis of the result that the recombinant domain showed equal ligand binding affinity and folding property as previously described [11], the spectrum was referred as correctly folded state of the domain. To further assess the state of folding of the synthetic δC1b domain, a molar equivalent of EDTA to zinc ion was added. The minimum absorption showed a blue-shift, indicating that the zinc ion plays an important role in the folding of the domain. Furthermore, the molecular weight of the folded domain with zinc ions was char acterized by ESI-MS [11]. The charge states of 4+ and 5+ (*m/z*: 1506.6 and 1205.5, respectively) were observed and their reconstructed mass (6023.4) was consistent with the calculated mass of

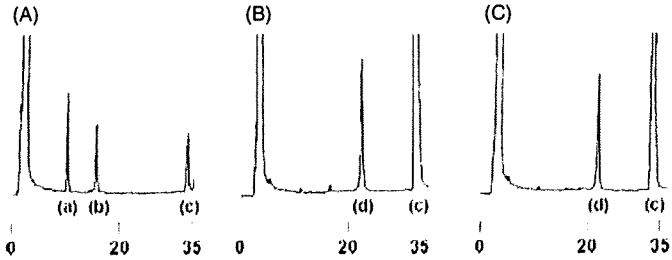

Figure 1. HPLC charts of the NCL reaction solution. Charts (A)–(C) show the reaction progress at 0, 6.5, and 18 h incubation, respectively, after the thiophenol addition. Numbers under each chart indicate the elution time (minutes). Peaks (a)–(d) show as follows: a, δC1b(231–246) (2-mercaptopropionate thioester); b, δC1b(247–281); c, thiophenol; d, δC1b(231–281).

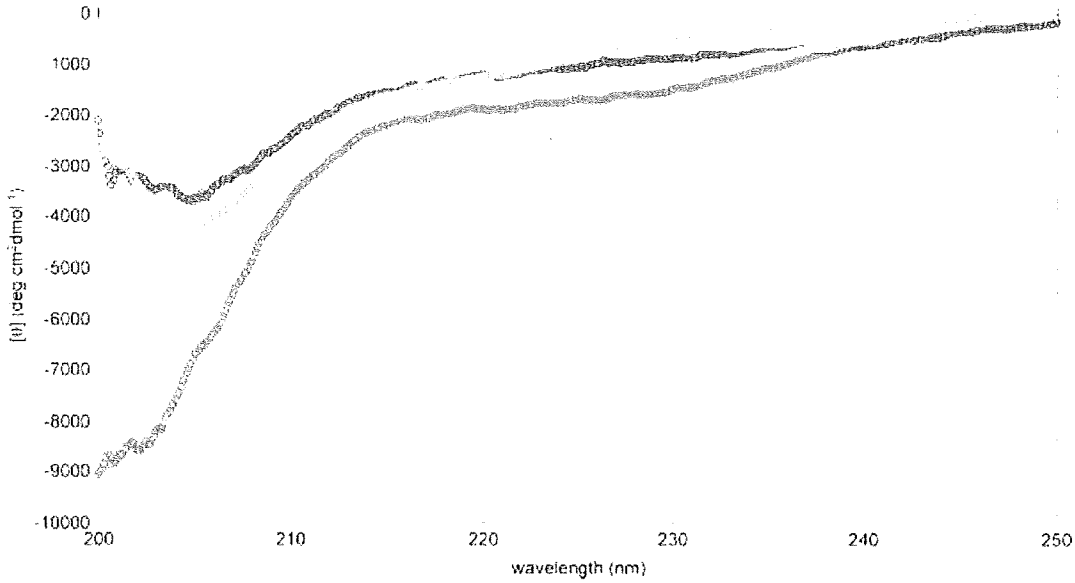

Figure 2. CD spectra of the synthetic δC1b peptide in the presence or absence of metals and comparison with that of a recombinant δC1b domain. The buffer contains 50 mM Tris·HCl (pH 7.5) and 1 mM DTT. Spectra shown are as follows: orange dots, peptide (50 μM) only; blue dots, peptide (50 μM) + 100 μM $ZnCl_2$; yellow dots, peptide (50 μM) + 100 μM $ZnCl_2$ + 100 μM EDTA; light blue dots, the recombinant δC1b domain.

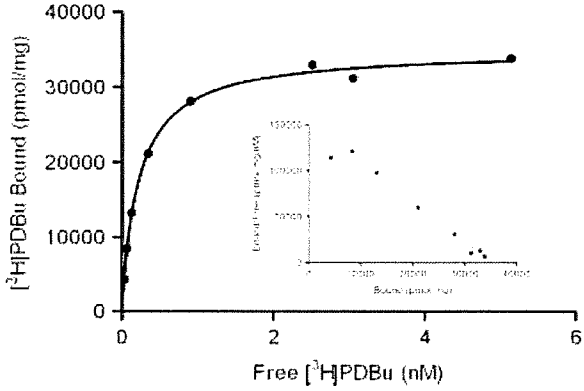

Figure 3. Representative saturation curves with increasing concentrations of [^{3}H]PDBu. [^{3}H]PDBu scatchard plots for the synthetic δC1b domain are shown in the panel. Binding was measured using the polyethylene glycol precipitation assay. Each point represents the mean of triplicate determinations, generally with a standard error of 2%. Similar results were obtained in two additional experiments.

δC1b(231 - 281) + 2Zn – 4H (6022.6) [21]. The ligand binding of the synthetic δC1b domain was assessed by binding assays utilizing [^{3}H]PDBu. The K_d for PDBu was determined to be 0.34 ± 0.08 nM (mean ± SEM, n = 3 experiments) (Figure 3). This value shows that the synthetic δC1b domain is comparable to the recombinant protein domain (K_d = 0.8 ± 0.1 nM) in ligand binding analyses [22].

Conclusions

In summary, a Cys-rich peptide, PKCδ C1b domain, was successfully synthesized by NCL methodology. In the synthesis of C1b domains by a stepwise condensation method, special reagents and resins such as HATU and PEG-PS resin were utilized on account of difficulty in coupling [11]. The fragment condensation by NCL would be an advantageous alternative method since normal reagents can be used for the synthesis of each fragment. Proper zinc-finger structure folding was determined by CD spectra. The binding of PDBu was assessed by polyethyleneglycol precipitation assays and the result indicated that the synthetic δC1b domain is suitable for use in ligand binding analyses. This methodology makes feasible the efficient preparation of modified C1b domains, which might be useful for the establishment of new binding assay methods or for the characterization of newly synthetic isozyme-specific ligands.

Acknowledgements

This work was supported in part by a Grant-in-aid from the Ministry of Education, Culture, Sports, Science, and Technology, Japan, and of the Ministry of Health, Labour, and Welfare. It was also supported in part by the Intramural Program of the National Institutes of Health, Center for Cancer Research, National Cancer Institute. The authors thank Professor Kazunari Akiyoshi, Institute of Biomaterials and Bioengineering, Tokyo Medical and Dental University, for his assistance in the CD experiments.

Supporting information

Supporting information may be found in the online version of this article.

References

1 Nishizuka Y. Intracellular signaling by hydrolysis of phospholipids and activation of protein kinase C. *Science* 1992; **11**: 607 - 614.
2 Newton AC. Protein kinase C: structure, function, and regulation. *J. Biol. Chem.* 1995; **270**: 28495 - 28498.
3 Watanabe T, Ono Y, Taniyama Y, Hazama K, Igarashi K, Ogita K, Kikkawa U, Nishizuka Y. Cell division arrest induced by phorbol ester in CHO cells overexpressing protein kinase C-delta subspecies. *Proc. Natl Acad. Sci. USA* 1992; **89**: 10159 10163.
4 Mischak H, Pierce JH, Goodnight J, Kazanietz G, Blumberg PM, Mushinski JF. Phorbol ester induced myeloid differentiation is

mediated by protein kinase C-alpha and -delta and not by protein kinase C-beta II, -epsilon, -zeta, and -eta. *J. Biol. Chem.* 1993; **268**: 20110–20115.

5 Li C, Wernig E, Leitges M, Hu Y, Xu Q. Mechanical stress-activated PKCδ regulates smooth muscle cell migration. *FASEB J.* 2003; **17**: 2106–2108.

6 Ghayur T, Hugunin M, Talanian V, Ratnofsky S, Quinlan C, Emoto Y, Pandey P, Datta R, Huang Y, Kharbanda S, Allen H, Kamen R, Wong W, Kufe D. Proteolytic activation of protein kinase C delta by an ICE/CED 3-like protease induces characteristics of apoptosis. *J. Exp. Med.* 1996; **184**: 2399–2404.

7 Humphries MJ, Limesand KH, Schneider JC, Nakayama KI, Anderson SM, Reyland ME. Suppression of apoptosis in the protein kinase Cδ null mouse in vivo. *J. Biol. Chem.* 2006; **281**: 9728–9737.

8 Tamamura H, Sigano DM, Lewin NE, Blumberg PM, Marquez VE. Conformationally constrained analogues of diacylglycerol. 20. The search for an elusive binding site on protein kinase C through relocation of the carbonyl pharmacophore along the sn-1 side chain of 1,2-diacylglycerol lactones. *J. Med. Chem.* 2004; **47**: 644–655.

9 Tamamura H, Sigano DM, Lewin NE, Peach ML, Nicklaus MC, Blumberg PM, Marquez VE. Conformationally constrained analogues of diacylglycerol (DAG). 23. Hydrophobic ligand-protein interactions versus ligand-lipid interactions of DAG-lactones with protein kinase C (PK-C). *J. Med. Chem.* 2004; **47**: 4858–4864.

10 Marquez VE, Blumberg PM. Synthetic diacylglycerols (DAG) and DAG-lactones as activators of protein kinase C (PK-C). *Acc. Chem. Res.* 2003; **36**: 434–443.

11 Irie K, Oie K, Nakahara A, Yanai Y, Ohigashi H, Wender PA, Fukuda H, Konishi H, Kikkawa U. Molecular basis for protein kinase C isozyme-selective binding: the synthesis, folding, and phorbol ester binding of the cysteine-rich domains of all protein kinase C isozymes. *J. Am. Chem. Soc.* 1998; **120**: 9159–9167.

12 Dawson PE, Muir TW, Clark-Lewis I, Kent SBH. Synthesis of proteins by native chemical ligation. *Science* 1994; **266**: 776–779.

13 Dawson PE, Churchill MJ, Ghadiri MR, Kent SBH. Modulation of reactivity in native chemical ligation through the use of thiol additives. *J. Am. Chem. Soc.* 1997; **119**: 4325–4329.

14 von Eggelkraut-Gottanka R, Klose A, Beck-Sickinger AG, Beyermann M. Peptide "thioester formation using standard Fmoc-chemistry. *Tetrahedron Lett.* 2003; **44**: 3551–3554.

15 Sharkey NA, Blumberg PM. Highly lipophilic phorbol esters as inhibitors of specific [3H]phorbol 12,13-dibutyrate binding. *Cancer Res.* 1985; **45**: 19–24.

16 Kazanietz MG, Krausz KW, Blumberg PM. Differential irreversible insertion of protein kinase C into phospholipid vesicles by phorbol esters and related activators. *J. Biol. Chem.* 1992; **267**: 20878–20886.

17 Kajihara Y, Yoshihara A, Hirano K, Yamamoto N. Convenient synthesis of a sialylglycopeptide-thioester having an intact and homogeneous complex-type disialyl-oligosaccharide. *Carbohydr. Res.* 2006; **341**: 1333–1340.

18 Futaki S, Tatsuto K, Shiraishi Y, Sugiura Y. Total synthesis of artificial zinc-finger protein. Problems and perspectives. *Biopolymers* 2004; **76**: 98–109.

19 Hackeng TM, Griffin JH, Dawson PE. Protein synthesis by native chemical ligation: expanded scope by using straightforward methodology. *Proc. Natl Acad. Sci. USA* 1999; **96**: 10068–10073.

20 Zhang G, Kazanietz MG, Blumberg PM, Hurley JH. Crystal structure of the cys2 activator-binding domain of protein kinase C delta in complex with phorbol ester. *Cell* 1995; **81**: 917–924.

21 Tamamura H, Otaka T, Murakami T, Ibuka T, Sakano K, Waki M, Matsumoto A, Yamamoto N, Fujii N. An anti-HIV peptide, T22, forms a highly active complex with Zn(II). *Biochem. Biophys. Res. Commun.* 1996; **229**: 648–652.

22 Kazanietz MG, Wang S, Milne GW, Lewin NE, Liu LH, Blumberg PM. Residues in the second cysteine-rich region of protein kinase C δ relevant to phorbol ester binding as revealed by site-directed mutagenesis. *J. Biol. Chem.* 1995; **270**: 21852–21859.

Bioorganic & Medicinal Chemistry Letters 20 (2010) 354–358

Contents lists available at ScienceDirect

Bioorganic & Medicinal Chemistry Letters

journal homepage: www.elsevier.com/locate/bmcl

CD4 mimics targeting the mechanism of HIV entry

Yuko Yamada [a], Chihiro Ochiai [a], Kazuhisa Yoshimura [b], Tomohiro Tanaka [a], Nami Ohashi [a], Tetsuo Narumi [a], Wataru Nomura [a], Shigeyoshi Harada [b], Shuzo Matsushita [b], Hirokazu Tamamura [a,*]

[a] Institute of Biomaterials and Bioengineering, Tokyo Medical and Dental University, Chiyoda-ku, Tokyo 101-0062, Japan
[b] Center for AIDS Research, Kumamoto University, Kumamoto 860-0811, Japan

ARTICLE INFO

Article history:
Received 19 September 2009
Revised 20 October 2009
Accepted 22 October 2009
Available online 4 November 2009

Keywords:
CD4 mimic
HIV entry
Synergistic effect
CXCR4

ABSTRACT

A structure–activity relationship study was conducted of several CD4 mimicking small molecules which block the interaction between HIV-1 gp120 and CD4. These CD4 mimics induce a conformational change in gp120, exposing its co-receptor-binding site. This induces a highly synergistic interaction in the use in combination with a co-receptor CXCR4 antagonist and reveals a pronounced effect on the dynamic supramolecular mechanism of HIV-1 entry.

Recently, remarkable success has attended the clinical treatment of HIV-infected and AIDS patients, with 'highly active antiretroviral therapy (HAART)'. This approach involves a combination of two or three agents from two categories: reverse transcriptase inhibitors and protease inhibitors.[1] In addition, the molecular mechanism involved in HIV-entry and -fusion into host cells has been described in detail.[2] The complex interactions of surface proteins on cellular and viral membranes, which are designated as a dynamic supramolecular mechanism of HIV entry, are reported to be crucial to the viral infection. In a first step, an HIV envelope protein, gp120 interacts with a cell surface protein, CD4, leading to a conformational change in gp120 followed by subsequent binding of gp120 to a co-receptor CCR5[3] or CXCR4.[4] CCR5 and CXCR4 are the major co-receptors for the entry of macrophage-tropic (R5-) and T cell line-tropic (X4-) HIV-1, respectively. The interaction of gp120 with CCR5 or CXCR4 triggers entry of another envelope protein, gp41 to the cell membrane and formation of a gp41 trimer-of-hairpins structure, which causes fusion of HIV/cell-membranes and completes the infection.

Informed by this mechanism, a fusion inhibitor, enfuvirtide (fuzeon, Trimers & Roche)[5] and a CCR5 antagonist, maraviroc (Pfizer)[6] in addition to an integrase inhibitor, raltegravir (Merck)[7] have been used clinically. However, serious problems with chemotherapy still persist, including the emergence of viral strains with multi-drug resistance (MDR), considerable adverse effects and high costs. Consequently, development of novel drugs possessing mechanisms of action different from those of the above inhibitors is currently required. We have previously developed selective CXCR4 antagonists[8] and fusion inhibitors.[9] Furthermore, *N*-(4-Bromophenyl)-*N'*-(2,2,6,6-tetramethylpiperidin-4-yl)-oxalamide (**1**) and *N*-(4-chlorophenyl)-*N'*-(2,2,6,6-tetramethylpiperidin-4-yl)-oxalamide (**2**) were previously found using chemical library screening to inhibit syncytium formation by other researchers.[10] **1** and **2** bind to gp120 with binding affinities of K_d = 2.2 μM and 3.7 μM, respectively, blocking the interaction of gp120 with CD4 in the first step of an HIV-1 entry. Thus, in the present study we focus on the development of CD4 mimics that can block the interaction between gp120 and CD4. We have investigated the effect of CD4 mimics on conformational changes of gp120 and on their use in combination use with a CXCR4 antagonist.

Initially, molecular modeling of compound **2** docked into gp120 was carried out using docking simulations performed by the FlexSIS module of SYBYL 7.1 (Tripos, St. Louis) (Fig. 1).[11] The atomic coordinates of the crystal structure of gp120 with soluble CD4 (sCD4) were retrieved from Protein Data Bank (PDB) (entry 1RZJ) (Fig. 1a) and it was observed that Phe^{43} and Arg^{59} of the CD4 have multiple contacts with Asp^{368}, Glu^{370} and Trp^{427} of gp120, which are all conserved residues. An inspection of the environment of compound **2** docked in gp120 revealed the presence of a large cavity around the *p*-position of the phenyl ring of compound **2**, which could interact with the viral surface protein gp120 (Fig. 1b and c). Several analogs of **2** with substituents on the phenyl ring were therefore synthesized.

All compounds except **12** were synthesized by previously published methods (Scheme 1).[10b,12,13] Aniline derivatives (**3**) were coupled with ethyl oxalyl chloride to yield the corresponding ethyl oxalamates **4**. Saponification of the above oxalamates to the corresponding free acids and the subsequent coupling with 4-ami-

* Corresponding author.
E-mail address: tamamura.mr@tmd.ac.jp (H. Tamamura).

0960-894X/$ - see front matter © 2009 Elsevier Ltd. All rights reserved.
doi:10.1016/j.bmcl.2009.10.098

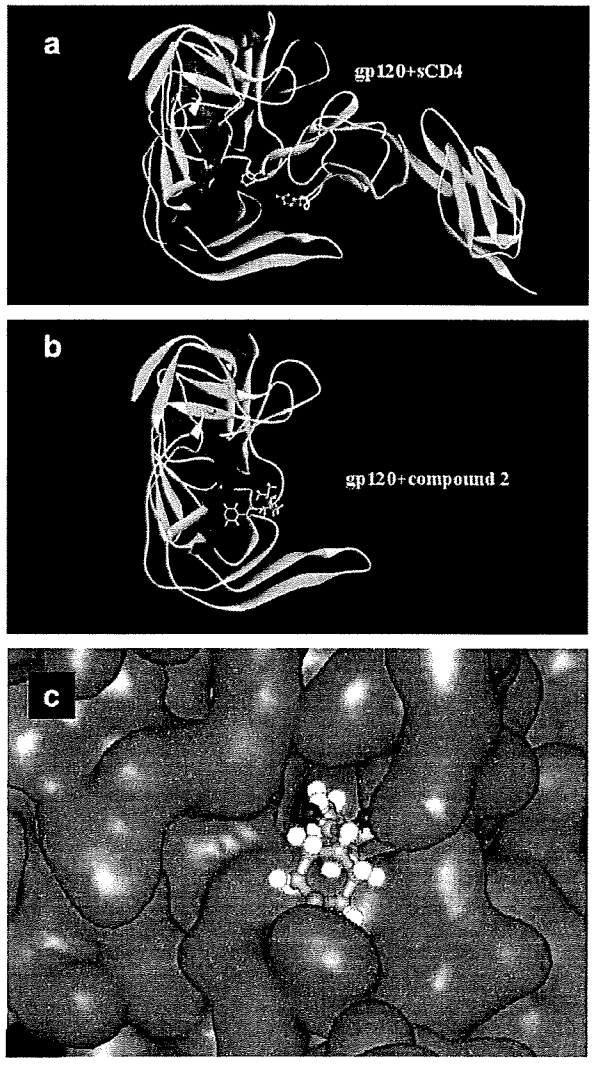

Figure 1. (a) The crystal structure of gp120 with soluble CD4 (sCD4) retrieved from the PDB (entry 1RZJ); (b) docking structure of compound **2** and gp120; (c) a focused figure of (b) shown by space-filling model.

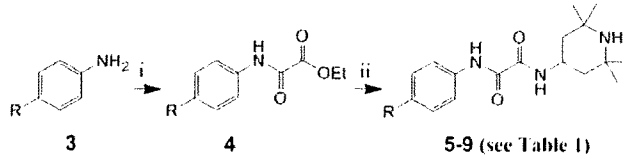

Scheme 1. Reagents and conditions: (i) ethyl oxalyl chloride, Et_3N; (ii) 1 M NaOH; 4-amino-2,2,6,6-tetramethylpiperidine, 1-(3-dimethylaminopropyl)-3-ethylcarbodiimide hydrochloride, 1-hydroxybenzotriazole, Et_3N.

no-2,2,6,6-tetramethylpiperidine using 1-ethyl-3-(3-dimethylaminopropyl)carbodiimide hydrochloride (EDC) and 1-hydroxybenzotriazole (HOBt) yielded compounds **5–9**. In the case of compound **12**, whose amide bond is not stable during the reaction of the saponification of the corresponding oxalamates, an alternative synthetic scheme was used (Scheme 2).[14] The reaction of *p*-nitroaniline (**10**) with oxalyl chloride gave the corresponding oxoacetamide **11**, which was subsequently coupled with 4-amino-2,2,6,6-tetramethylpiperidine to yield the desired compound **12**.

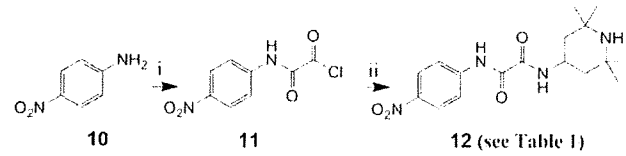

Scheme 2. Reagents and conditions: (i) oxalyl chloride, Et_3N; (ii) 4-amino-2,2,6,6-tetramethylpiperidine, Et_3N.

The anti-HIV activity of the synthetic compounds was evaluated against various viral strains including both laboratory and primary isolates (Table 1). IC_{50} values were determined by the 3-(4,5-dimethylthiazol-2-yl)-2,5-diphenyltetrazolium bromide (MTT) method[15] as the concentrations of the compounds which conferred 50% protection against HIV-1-induced cytopathogenicity in PM1/CCR5 cells. Cytotoxicity of the compounds based on the viability of mock-infected PM1/CCR5 cells was also evaluated using the MTT method. CC_{50} values were determined as the concentrations achieving 50% reduction of the viability of mock-infected cells. Compounds **1** and **2** showed potent anti-HIV activity against laboratory isolates, IIIB (X4, Sub B) and 89.6 (dual, Sub B) strains, and compound **2** also possessed potent activity against a primary isolate, an fTOI strain (R5, Sub B). All of the IC_{50} values were between 4 μM and 10 μM. Compound **1** was not tested against primary isolates. The potencies of compounds **1** and **2** are comparable to the reported binding affinities for gp120 (K_d = 2.2 and 3.7 μM, respectively).[10] Several of the new analogs of compounds **1** and **2** showed significant anti-HIV activity. Compound **5**, which has a phenyl group in place of the *p*-chlorophenyl group of compound **2**, did not show significant anti-HIV activity at concentrations below 100 μM against all strains tested except for an fTOI strain (R5, Sub B). This result suggests that a substituent at the *p*-position of the phenyl ring is critical for potent activity. Compound **6**, which has a fluorine atom at the *p*-position of the phenyl ring, showed moderate anti-HIV activity against laboratory isolates, IIIB (X4, Sub B) and 89.6 (dual, Sub B) strains (IC_{50} = 61 and 81 μM, respectively), but, at concentrations below 100 μM, failed to show significant anti-HIV activity against a primary isolate, a KYAG strain (R5, Sub B). Among halogen atoms, fluorine is less suitable than bromine or chlorine as a substituent at the *p*-position of the phenyl ring, as evidenced by compound **6**, which is 8–15-fold less potent than compounds **1** and **2** against IIIB (X4, Sub B) and 89.6 (dual, Sub B) strains. Compound **7**, which has a methyl group at the *p*-position of the phenyl ring, showed relatively more potent activity against IIIB (X4, Sub B) and 89.6 (dual, Sub B) strains (IC_{50} = 23 and 41 μM, respectively) than compound **6**. Compound **7** also showed significant anti-HIV activity against primary isolates, fTOI (R5, Sub B) and KYAG (R5, Sub B) strains (IC_{50} = 16 and 51 μM, respectively). Compound **8**, with a methoxy group at the *p*-position of the phenyl ring, did not show significant anti-HIV activity against all strains tested until a concentration of 100 μM was reached. In the biological assays, derivatives having electron-withdrawing substituents such as bromine, chlorine and fluorine at the *p*-position of the phenyl ring are relatively potent, whereas derivatives having electron-donating groups such as methoxy at this position are not potent. Furthermore, the steric effect of a substituent at the *p*-position of the phenyl ring appears to be critical to anti-HIV activity. The sum of Hammett constants (σ) of benzoic acid substituents[16] shown in Table 1 can be used to evaluate the electron-withdrawing or -donating effect of the substituents on the aromatic ring. The Taft E_s values[16a,17] were used as steric parameters for substituents at the *p*-position of the phenyl ring. The order of potency found for the halogen-containing derivatives in anti-HIV activity against laboratory isolates, IIIB (X4, Sub B) and 89.6 (dual, Sub B), is: compound **1** (R = Br) (σ = 0.23, E_s = −1.16), **2**

Table 1
Hammett constants (σ) and steric effects (E_s) of substituted aromatic rings and anti-HIV activity and cytotoxicity of synthetic compounds

Compd	R[a]	σ[b]	E_s[c]	IC_{50}[e] (μM)				CC_{50}[e] (μM)
				Lab. isolates		Primary isolates		
				IIIB (X4)	89.6 (dual)	fTOI (R5)	KYAG (R5)	
1	Br	0.23	−1.16	4	9	ND	ND	150
2	Cl	0.23	−0.97	8	10	5	>30	170
5	H	0	0	>100	>100	81	>100	350
6	F	0.06	−0.46	61	81	ND	>100	320
7	CH_3	−0.17	−1.24	23	41	16	51	210
8	OCH_3	−0.27	−0.55	>100	>100	ND	>100	340
9	CF_3	0.54	−2.40	ND	27	ND	ND	72
12	NO_2	0.78	−1.77[d]	ND	42	ND	ND	230
sCD4				0.010	0.021	0.0044	ND	ND

[a] See Schemes 1 and 2.
[b] σ = Hammett constant of a substitutent on a benzoic acid derivative.[16]
[c] E_s = steric effect of a substituent at the *para* position on the aromatic ring.[16a,17]
[d] The average value of −1.01 and −2.52, which are E_s values of the NO_2 group, −1.77, was used.
[e] Values are means of at least three experiments (ND = not determined).

(R = Cl) (σ = 0.23, E_s = −0.97), **6** (R = F) (σ = 0.06, E_s = −0.46) and **5** (R = H) (σ = 0, E_s = 0). This is the order of substituents' electron-withdrawing ability and also of their size. Methyl (σ = −0.17, E_s = −1.24) is an electron-donating group, but is almost as bulky as a bromine atom. Thus, the *p*-methyl derivative **7** has relatively potent anti-HIV activity against laboratory isolates, IIIB (X4, Sub B) and 89.6 (dual, Sub B), higher than that of compound **6** (R = F) but lower than that of compound **1** (R = Br) or **2** (R = Cl). The electron-donating ability of a methoxy group is stronger (σ = −0.27), but the bulk size is smaller (E_s = −0.55), than that of a methyl group. Thus, the *p*-methoxy derivative **8** has no significant anti-HIV activity against all strains tested at concentrations below 100 μM. Two derivatives containing bulkier and more potent electron-withdrawing substituents such as trifluoromethyl (R = CF_3) (σ = 0.54, E_s = −2.40) and nitro (R = NO_2) (σ = 0.78, E_s = −1.77) at the *p*-position of the phenyl ring were evaluated. Compounds **9** (R = CF_3) and **12** (R = NO_2) showed significant anti-HIV activity against an 89.6 (dual, Sub B) strain. These are less potent than compounds **1** and **2** and this is perhaps due to the excessive size of the substituents at the *p*-position. This suggests that a certain level of the bulk size and a potent electron-withdrawing ability of the substituents are preferable for anti-HIV activity. It is estimated that a cavity around the *p*-position of the phenyl ring of CD4 mimicking compounds would be optimally filled by bromine (E_s = −1.16) or a methyl group (E_s = −1.24) at *p*-position, and that an electron-deficient aromatic ring might interact tightly with a negatively charged group such as carboxy of Glu^{370}. In isothermal titration calorimetry (ITC) experiments reported elsewhere,[10c] compound **5** (R = H) does not have significant affinity for gp120, and compound **6** (R = F) has less potent affinity for gp120 than compound **2**, consistent with the present data. In all but one of the compounds, no significant cytotoxicity was detected (CC_{50} >150 μM, Table 1), the exception being compound **9** (R = CF_3) (CC_{50} = 72 μM). Compounds **7** and **12** have relatively low cytotoxicities, compared to compounds **1** and **2**.

Fluorescence activated cell sorting (FACS) analysis was performed[15] to investigate whether these synthetic compounds interact with gp120 inducing the conformational change necessary for the approach of an anti-envelope antibody or a co-receptor to the gp120. The profile of binding of an anti-envelope CD4-induced monoclonal antibody, 4C11, to the Env-expressing cell surface (an R5-HIV-1 strain, JR-FL,-infected PM1 cells) pretreated with the above CD4 mimic analogs was examined. Comparison of the binding of 4C11 to the cell surface was measured in terms of the mean fluorescence intensity (MFI), and is shown in Figure 2. Pretreatment of the Env-expressing cells with compound **2** (MFI = 38.42) produced a remarkable increase in binding affinity for 4C11, similar to that observed in pretreatment with sCD4 (MFI = 37.90). This is consistent with the results in the previous paper[10] where it was reported that compound **2** enhances the binding of gp120 to the 17b monoclonal antibody which recognizes the co-receptor binding site of gp120. Env-expressing cells, which were not pretreated with sCD4 or a CD4 mimic compound, did not show significant binding affinity for 4C11 (Fig. 2, blank). The increase in binding affinity for monoclonal antibodies may be due to conformational changes in gp120, which were caused by the interaction of sCD4 or a CD4 mimic with gp120. It is hypothesized that such conformational changes involve the exposure of the co-receptor binding site of gp120 (the V3 loop), which is hidden internally, since the binding of gp120 to 17b is enhanced. Compound **5**, which failed to show significant anti-HIV activity, and compounds **7**, **9** and **12**, which had significant anti-HIV activity, were assessed in the FACS analysis. The profile of the binding of 4C11 to the Env-expressing cell surface pretreated with compound **5** (MFI = 14.34) was similar to that of the blank (MFI = 11.24), suggesting that compound **5** offers no significant enhancement of binding affinity for 4C11. This result is compatible with the anti-HIV activity of compound **5**. The profile of the binding of 4C11 to the Env-expressing cell surface pretreated with compound **7** (MFI = 38.33) was entirely similar to that of compound **2** used as a pretreatment. Pretreatment of the cell surface with compounds **9** and **12** (MFI = 29.09 and 30.01, respectively) produced a slightly lower enhancement of binding affinity for 4C11, compared to those of compounds **2** and **7** as pretreatments. However, in the ITC experiments reported elsewhere,[10c] compound **9** (R = CF_3) has a high affinity for gp120, comparable to that of compound **2**, but compound **12** (R = NO_2) does not have significant affinity for gp120, indicating that these are not consistent with the current FACS studies, possibly due to the difference in the assay systems. Although the anti-HIV activity of **7** is weaker than that of compound **2**, the level of compound **7** inducing an enhancement of binding affinity of gp120 for 4C11 is comparable to that of compound **2**. The concentration of compounds used in the FACS analysis was 100 μM, much beyond the IC_{50} values of compounds **2** and **7**. A concentration of 100 μM would be also sufficient for the expression of anti-HIV activity caused by compounds **2** and **7**.

An effect on the use of compound **2** combined with another entry inhibitor was investigated. Analysis of the synergistic effects of anti-HIV agents was performed according to the median effect principle using the CalcuSyn version 2 computer program[18] to estimate IC_{50} values of compounds in different combinations. Combination indices (CI) were estimated from the data evaluated using the MTT assay

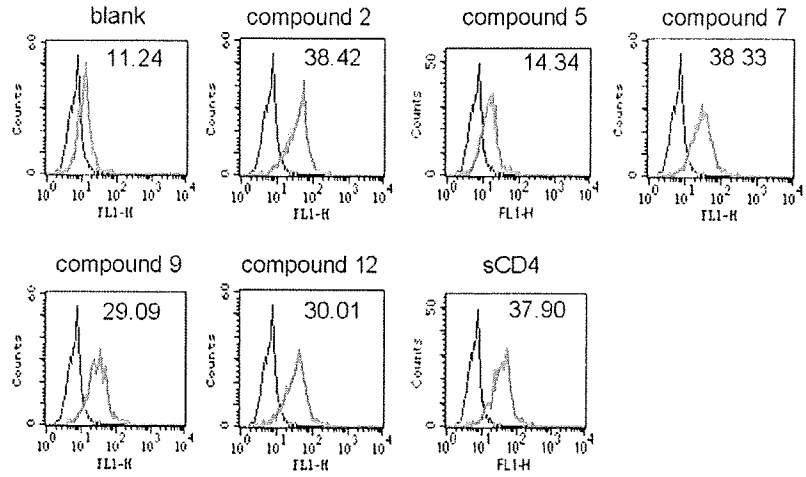

Figure 2. JR-FL (R5, Sub B) chronically infected PM1 cells were preincubated with 100 μM of a CD4 mimic or sCD4 (11 nM) for 15 min, and then incubated with an anti-HIV-1 mAb, 4C11, at 4 °C for 15 min. The cells were washed with PBS, and fluorescein isothiocyanate (FITC)-conjugated goat anti-human IgG antibody was used for antibody-staining. Flow cytometry data for the binding of 4C11 (green lines) to the Env-expressing cell surface in the presence of sCD4 or a CD4 mimic are shown among gated PM1 cells along with a control antibody (anti-human CD19: black lines). Data are representative of the results from a minimum of two independent experiments. The number at the top of each graph shows the mean fluorescence intensity (MFI) of the antibody 4C11.

Table 2
Combination indices (CI) for compound **2** or sCD4 and a CXCR4 antagonist, T140, against an HIV IIIB strain

Combination	HIV strain	CI values at different IC[a]		
		IC_{50}	IC_{75}	IC_{90}
2 + T140	IIIB	0.786	0.713	0.655
sCD4 + T140	IIIB	0.705	0.528	0.400

[a] The multiple-drug effect analysis reported by Chou et al. was used to analyze the effects of combinational uses of compounds.[18] CI <0.9: synergy, 0.9 < CI < 1.1: additivity, CI >1.1: antagonism.

(Table 2).[15] Compound **2** showed a highly remarkable synergistic anti-HIV activity with a co-receptor CXCR4 antagonist, T140,[8a] against an X4-HIV-1 strain, IIIB at various IC values (IC_{50}, IC_{75} and IC_{90}). However, sCD4 exhibited a higher synergistic effect (lower CI values) with T140 (Table 2). The interaction of sCD4 or a CD4 mimic with gp120 would expose the co-receptor-binding site of gp120, and the co-receptor CXCR4 could then easily approach gp120. Thus, an inhibitory effect of a CXCR4 antagonist would be meaningful, and a significant synergistic effect might also be brought about by a combination of sCD4 or a CD4 mimic and T140.

In summary, a series of CD4 mimic compounds were synthesized and evaluated for their anti-HIV activity. Several compounds showed significant anti-HIV activity with relatively low cytotoxicity. SAR studies showed that a certain level of size and electron-withdrawing ability of the substituents at the *p*-position of the phenyl ring are suitable for potent anti-HIV activity. In addition, the treatment of Env-expressing cells with several CD4 mimicking compounds causes a conformational change, exposing the co-receptor-binding site of gp120 externally. Thus, a CD4 mimic exhibited a remarkable synergistic effect with a co-receptor antagonist. These compounds are essential probes directed to the dynamic supramolecular mechanism of HIV entry, and important leads for the cocktail therapy of AIDS.

Acknowledgments

This work was supported by Mitsui Life Social Welfare Foundation, Grant-in-Aid for Scientific Research from the Ministry of Education, Culture, Sports, Science, and Technology of Japan, and Health and Labour Sciences Research Grants from Japanese Ministry of Health, Labor, and Welfare.

References and notes

1. Mitsuya, H.; Erickson, J. In *Textbook of AIDS Medicine*; Merigan, T. C., Bartlett, J. G., Bolognesi, D., Eds.; Williams & Wilkins: Baltimore, 1999; pp 751–780.
2. Chan, D. C.; Kim, P. S. *Cell* **1998**, *93*, 681.
3. (a) Alkhatib, G.; Combadiere, C.; Broder, C. C.; Feng, Y.; Kennedy, P. E.; Murphy, P. M.; Berger, E. A. *Science* **1996**, *272*, 1955; (b) Choe, H.; Farzan, M.; Sun, Y.; Sullivan, N.; Rollins, B.; Ponath, P. D.; Wu, L.; Mackay, C. R.; LaRosa, G.; Newman, W.; Gerard, N.; Gerard, C.; Sodroski, J. *Cell* **1996**, *85*, 1135; (c) Deng, H. K.; Liu, R.; Ellmeier, W.; Choe, S.; Unutmaz, D.; Burkhart, M.; Marzio, P. D.; Marmon, S.; Sutton, R. E.; Hill, C. M.; Davis, C. B.; Peiper, S. C.; Schall, T. J.; Littman, D. R.; Landau, N. R. *Nature* **1996**, *381*, 661; (d) Doranz, B. J.; Rucker, J.; Yi, Y. J.; Smyth, R. J.; Samson, M.; Peiper, S. C.; Parmentier, M.; Collman, R. G.; Doms, R. W. *Cell* **1996**, *85*, 1149; (e) Dragic, T.; Litwin, V.; Allaway, G. P.; Martin, S. R.; Huang, Y.; Nagashima, K. A.; Cayanan, C.; Maddon, P. J.; Koup, R. A.; Moore, J. P.; Paxton, W. A. *Nature* **1996**, *381*, 667.
4. Feng, Y.; Broder, C. C.; Kennedy, P. E.; Berger, E. A. *Science* **1996**, *272*, 872.
5. Wild, C. T.; Greenwell, T. K.; Matthews, T. J. *AIDS Res. Hum. Retroviruses* **1993**, *9*, 1051.
6. (a) Dorr, P.; Westby, M.; Dobbs, S.; Griffin, P.; Irvine, B.; Macartney, M.; Mori, J.; Rickett, G.; Smith-Burchnell, C.; Napier, C.; Webster, R.; Armour, D.; Price, D.; Stammen, B.; Wood, A.; Perros, M. *Antimicrob. Agents Chemother.* **2005**, *49*, 4721; (b) Price, D. A.; Armour, D.; De Groot, M.; Leishman, D.; Napier, C.; Perros, M.; Stammen, B. L.; Wood, A. *Bioorg. Med. Chem. Lett.* **2006**, *16*, 4633.
7. (a) Cahn, P.; Sued, O. *Lancet* **2007**, *369*, 1235; (b) Grinsztejn, B.; Nguyen, B.-Y.; Katlama, C.; Gatell, J. M.; Lazzarin, A.; Vittecoq, D.; Gonzalez, C. J.; Chen, J.; Harvey, C. M.; Isaacs, R. D. *Lancet* **2007**, *369*, 1261.
8. (a) Tamamura, H.; Xu, Y.; Hattori, T.; Zhang, X.; Arakaki, R.; Kanbara, K.; Omagari, A.; Otaka, A.; Ibuka, T.; Yamamoto, N.; Nakashima, H.; Fujii, N. *Biochem. Biophys. Res. Commun.* **1998**, *253*, 877; (b) Fujii, N.; Oishi, S.; Hiramatsu, K.; Araki, T.; Ueda, S.; Tamamura, H.; Otaka, A.; Kusano, S.; Terakubo, S.; Nakashima, H.; Broach, J. A.; Trent, J. O.; Wang, Z.; Peiper, S. C. *Angew. Chem., Int. Ed.* **2003**, *42*, 3251; (c) Tanaka, T.; Nomura, W.; Narumi, T.; Esaka, A.; Oishi, S.; Ohashi, N.; Itotani, K.; Evans, B. J.; Wang, Z.; Peiper, S. C.; Fujii, N.; Tamamura, H. *Org. Biomol. Chem.* **2009**, *7*, 3805.
9. Otaka, A.; Nakamura, M.; Nameki, D.; Kodama, E.; Uchiyama, S.; Nakamura, S.; Nakano, H.; Tamamura, H.; Kobayashi, Y.; Matsuoka, M.; Fujii, N. *Angew. Chem., Int. Ed.* **2002**, *41*, 2937.
10. (a) Zhao, Q.; Ma, L.; Jiang, S.; Lu, H.; Liu, S.; He, Y.; Strick, N.; Neamati, N.; Debnath, A. K. *Virology* **2005**, *339*, 213; (b) Schön, A.; Madani, N.; Klein, J. C.; Hubicki, A.; Ng, D.; Yang, X.; Smith, A. B., III; Sodroski, J.; Freire, E. *Biochemistry* **2006**, *45*, 10973; (c) Madani, N.; Schön, A.; Princiotto, A. M.; LaLonde, J. M.; Courter, J. R.; Soeta, T.; Ng, D.; Wang, L.; Brower, E. T.; Xiang, S.-H.; Do Kwon, Y.; Huang, C.-C.; Wyatt, R.; Kwong, P. D.; Freire, E.; Smith, A. B., III; Sodroski, J. *Structure* **2008**, *16*, 1689; (d) Haim, H.; Si, Z.; Madani, N.; Wang, L.; Courter, J. R.; Princiotto, A.; Kassa, A.; DeGrace, M.; McGee-Estrada, K.; Mefford, M.; Gabuzda, D.; Smith, A. B., III; Sodroski, J. *ProS Pathogens* **2009**, *5*, 1.
11. The structure of compound **2** was built in Sybyl and minimized with the MMFF94 force field and partial charges. (see: Halgren, T. A. *J. Comput. Chem.* **1996**, *17*, 490.) Docking was then performed using FlexSIS through its SYBYL

module, into the crystal structure of gp120 (PDB, entry 1RZJ). The binding site was defined as residues Val^{255}, Asp^{368}, Glu^{370}, Ser^{375}, Ile^{424}, Trp^{427}, Val^{430} and Val^{475}, and included residues located within a radius 4.4 Å. The ligand was considered to be flexible, and all other options were set to their default values. Figures were generated with ViewerLite version 5.0 (Accelrys Inc., San Diego, CA).

12. *For example, the synthesis of compound* **7**: To a solution of ethyl oxalyl chloride (0.400 mL, 3.48 mmol) in THF (20 mL) were added triethylamine (Et_3N) (0.480 mL, 3.48 mmol) and *p*-toluidine (373 mg, 3.48 mmol) with stirring at 0 °C. The reaction mixture was allowed to warm to room temperature, and then stirred for 6 h. After removal by filtration of the resulting salts, the filtrate was concentrated under reduced pressure. The residue was extracted with EtOAc (50 mL), and the extract was washed successively with brine (20 mL), 1 M HCl (20 mL × 2), brine (20 mL), saturated $NaHCO_3$ (20 mL × 2) and brine (20 mL × 3), then dried over $MgSO_4$. Concentration under reduced pressure gave the crude ethyl oxalamate, which was used without further purification. To a solution of the crude ethyl oxalamate (640 mg, 3.09 mmol) in THF (30 mL) were added aqueous 1 M NaOH (3.40 mL, 3.40 mmol), water (50 mL) and MeOH (20 mL) with stirring at 0 °C. The reaction mixture was allowed to warm to room temperature, and then stirred for 20 h. After the addition of aqueous 1 M HCl (5 mL), MeOH and THF were evaporated under reduced pressure. The residue was acidified to pH 2 with 1 M HCl, and extracted with EtOAc (50 mL × 2). The combined organic layer was washed with brine (20 mL × 3), and dried over $MgSO_4$. Concentration under reduced pressure gave the crude acid, which was used for the next reaction without further purification. To a solution of the above crude acid (514 mg, 2.87 mmol) in THF (10 mL) were added 1-hydoxybenzotriazole (484 mg, 3.16 mmol), 4-amino-2,2,6,6-tetramethylpiperidine (446 μL, 2.58 mmol), 1-ethyl-3-(3-dimethylaminopropyl)carbodiimide hydrochloride (606 mg, 3.16 mmol) and Et_3N (0.439 mL, 3.16 mmol) with stirring at 0 °C. The reaction mixture was allowed to warm to room temperature, and then stirred for 20 h. After evaporation of THF, the residue was dissolved in $CHCl_3$ (50 mL). The mixture was washed with saturated $NaHCO_3$ (20 mL × 2) and brine (20 mL × 3), and dried over $MgSO_4$. Concentration under reduced pressure gave the crude crystalline mass. The usual work-up followed by recrystallization from EtOAc–*n*-hexane gave the title compound **7** (363 mg, 1.14 mmol, 39.8%) as colorless crystals, mp = 176 °C; δ_H (400 MHz; $CDCl_3$) 1.07 (1H, m, NH), 1.16 (6H, s, CH_3), 1.29 (6H, s, CH_3), 1.44 (2H, m, CH_2), 1.91 (1H, d, *J* 3.7, C*H*H), 1.94 (1H, d, *J* 3.7, CH*H*), 2.34 (3H, s, CH_3), 4.25 (1H, m, CH), 7.17 (2H, d, *J* 8.3, ArH), 7.33 (1H, m, NH), 7.50 (2H, d, *J* 8.4, ArH), 9.18 (1H, s, NH); HRMS (FAB), *m/z* calcd for $C_{18}H_{28}N_3O_2$ $(MH)^+$ 318.2182, found 318.2173.
13. McFarland, C.; Vicic, D. A.; Debnath, A. K. *Synthesis* **2006**, 807.
14. *The synthesis of compound* **12**: To a solution of Et_3N (417 μL, 3.00 mmol) and 4-nitroaniline (138 mg, 1.00 mmol) in THF (1.3 mL) was added oxalyl dichloride (85.8 μL, 1.00 mmol) with stirring at 0 °C. After being stirred for 30 min at 0 °C, Et_3N (167 μL, 1.20 mmol) and 4-amino-2,2,6,6-tetramethylpiperidine (156 μL, 0.90 mmol) were added. The reaction mixture was stirred for 6 h at 0 °C. After removal by filtration of the resulting salts, the filtrate was concentrated under reduced pressure. The residue was dissolved in $CHCl_3$ (20 mL), and the mixture was washed successively with brine (10 mL), saturated $NaHCO_3$ (10 mL × 2) and brine (10 mL × 3), and dried over $MgSO_4$. Concentration under reduced pressure followed by flash chromatography over silica gel with $CHCl_3$–MeOH (9:1) gave 42.4 mg (0.122 mmol, 13.5%) of the title compound **12** as colorless crystals, mp = 190 °C; δ_H (400 MHz; $CDCl_3$) 1.09 (1H, m, NH), 1.17 (6H, s, CH_3), 1.29 (6H, s, CH_3), 1.43 (2H, m, CH_2), 1.92 (1H, d, *J* 3.8, C*H*H), 1.95 (1H, d, *J* 3.8, CH*H*), 4.28 (1H, m, CH), 7.29 (1H, m, NH), 7.82 (2H, d, *J* 9.1, ArH), 8.28 (2H, d, *J* 9.1, ArH), 9.55 (1H, s, NH); HRMS (FAB), *m/z* calcd for $C_{17}H_{25}N_4O_4$ $(MH)^+$ 349.1876, found 349.1871.
15. Yoshimura, K.; Shibata, J.; Kimura, T.; Honda, A.; Maeda, Y.; Koito, A.; Murakami, T.; Mitsuya, H.; Matsushita, S. *AIDS* **2006**, *20*, 2065.
16. (a) Chapman, N. B.; Shorter, J. *Advances in Linear Free Energy Relationship*; Plenum Press: London, 1972; (b) Chapman, N. B.; Shorter, J. *Correlation Analysis in Chemistry*; Plenum Press: London, 1978; (c) Hansch, C.; Leo, A. J.; Hoekman, D. *Exploring QSAR, Hydrophobic, Electronic, and Steric Constants*; American Chemical Society: Washington, DC, 1995.
17. Taft, R. W. In *Steric Effects in Organic Chemistry*; Newman, M. S., Ed.; John Wiley: New York, 1956; p 556.
18. (a) Chou, T. C.; Talalay, P. *J. Biol. Chem.* **1977**, *252*, 6438; (b) Chou, T. C.; Hayball, M. P. *CalcuSyn*, 2nd ed.; Biosoft: Cambridge, UK, 1996.

ELSEVIER

INSTITUT PASTEUR

Microbes and Infection 11 (2009) 964–972

www.elsevier.com/locate/micinf

Original article

Functional analysis of Foxp3 and CTLA-4 expressing HTLV-1-infected cells in a rat model

Ryo Takayanagi, Takashi Ohashi, Hisatoshi Shida*

Department of Molecular Virology, Institute for Genetic Medicine, Hokkaido University, Kita-ku, Sapporo, Hokkaido 060-0815, Japan

Received 24 February 2009; accepted 30 June 2009
Available online 19 July 2009

Abstract

Human T-cell leukemia virus type 1 (HTLV-1) is the etiologic agent of adult T-cell leukemia (ATL). Some ATL cells express Foxp3, which is known as regulatory T cell (Treg cell) specific transcription factor. It is suggested that Treg cell like suppressive activity of Foxp3 expressing ATL cells is associated to ATL development and related immunodeficiency. To develop an HTLV-1 model system that enables to investigate the association of Treg function in ATL progression, we examined the expression of Foxp3 and CTLA-4, Treg cell-associated factor, in established HTLV-1-infected rat cell lines and their regulatory function. We found the expression of Foxp3 in 10 of 22 and CTLA-4 in 10 of 19 HTLV-1-infected rat cell lines. Moreover, some of the Foxp3 and/or CTLA-4 expressing cell lines suppressed proliferation of naïve T cells that were stimulated with anti-CD3 antibody. Particularly all Foxp3$^+$ CTLA-4$^+$ cells showed the suppressive activity. Our data suggest the usefulness of our rat model systems for further analysis of the role of Treg cell-associated factors on the development of ATL and related immunodeficiency *in vivo*.

Keywords: HTLV-1; ATL; Foxp3; CTLA-4; Animal model

1. Introduction

Natural regulatory T cell (Treg cell) was identified as the CD4$^+$ CD25$^+$ Foxp3$^+$ T cell population that was developed in thymus [1]. Treg cells suppress the proliferation of TCR-activated naïve T cells so that this function contributes to maintain immune self-tolerance by suppressing self-reactive T cells. It has been reported that Treg cells use several suppressive mechanisms such as cell contact dependent suppression, regulatory cytokines and Granzyme B and perforin-mediated cytotoxicity depending on the circumstances of their surroundings [1,2]. Foxp3 has been generally agreed to be a crucial transcription factor that regulates the functions and development of the Treg cells. Exogenous expression of the *Foxp3* gene can convert naïve CD4$^+$CD25$^-$ T cells into CD4$^+$ CD25$^+$ regulatory T like cells, and induce Treg cell associated molecules, such as cytotoxic T lymphocyte antigen 4 (CTLA-4) [3]. CTLA-4 is constitutively expressed on Treg cells [4], but its involvement in the suppressive activity of Treg cells has been under debate [5,6]. Recently CTLA-4 activity for Treg suppressive function *in vivo* and *in vitro* has been demonstrated using Treg specific CTLA-4 conditional knockout (KO) mouse [7].

Adult T cell leukemia (ATL) is neoplastic disease etiologically linked to Human T cell leukemia virus type 1(HTLV-1). ATL patient causes immunodeficiency associated with defective cellular immunity [8,9]. Most of ATL cells exhibit CD4$^+$ CD25$^+$ T cell phenotype. Several group analyzed the relationship of the ATL cells with Treg cells to explain the reasons for the immunodeficiency in ATL patients. Some ATL cells and HTLV-1-infected human cells express Foxp3 and related molecules, such as CTLA-4 and GITR [10–13]. Moreover, some ATL cells have been reported to suppress T cell proliferation like T reg cells, suggesting the association of

* Corresponding author. Tel./fax: +81 11 706 7543.
E-mail address: hshida@igm.hokudai.ac.jp (H. Shida).

1286-4579/$ - see front matter © 2009 Elsevier Masson SAS. All rights reserved.
doi:10.1016/j.micinf.2009.06.007

Foxp3 expression with the immune escape of ATL cells and immunodeficiency [14].

To analyze the contribution of Foxp3 and Treg associated molecules to development of ATL in more detail, suitable animal model is required. Previously, we established various rat models for HTLV-1 infection including inbred and immunocompromised rats, which allowed the investigation about the ability of T cells to suppress HTLV-1-realted malignancy [15,16]. Moreover, we identified CRM1, a cellular cofactor of Rex that exports viral mRNA from the nucleus to the cytoplasm, to be a major factor, which restricts efficient replication of HTLV-1 in rats [17–19]. Human CRM1 (hCRM1) transgenic (Tg) rat supports replication of HTLV-1 in T cells at the level similar to human T cells *ex vivo* [20].

Since some of the rat HTLV-1-infected cell lines, which we previously established from CRM1 Tg and Wt rats, express CD25, the viral proteins [20], and possess tumorigenic potency [15], it is interesting to characterize the HTLV-1$^+$ rat cells in relation to Foxp3 and Treg cell associated molecules. In this paper, we report Foxp3 and CTLA-4 expression in the HTVL-1-infected rat cell lines for the first time. Moreover some of these cells showed Treg cell like activity that suppresses the proliferation of naïve T cells, which were stimulated through T cell receptor. Our data that indicate the functional similarity between Foxp3 and/or CTLA-4 expressing HTLV-1-infected rat cell lines and human ATL cells suggest the usefulness of our rat model systems for further analysis of Foxp3 and CTLA-4 contribution to development of ATL and related immunodeficiency.

2. Materials and methods

2.1. Cells

HTLV-1-immortalized cell lines from Wt or Tg rats were established by cocultivating thymocytes or splenocytes with human HTLV-1 producing cell line MT-2, which had been treated with 50 μg/ml of mitomycin C containing medium for 30 min at 37 °C. These cells were maintained in the medium supplemented with 10 U/ml of interleukin (IL)-2 (PEPROTECH EC) at the beginning of co-culture. Some cell lines were eventually freed from exogenous IL-2 [15]. We noted "(+)" or "(-)" following cell line names to distinguish IL-2 dependent or independent stage of each cell line. The HTLV-1-infected rat T cell line FPM1 BP [16] has been described previously.

2.2. Western blotting

Cells were lysed in ice-cold extraction buffer (10 mM Tris–HCl [pH 7.4], 1 mM $MgCl_2$, 0.5% NP-40) containing protease inhibitor cocktail (Complete mini; Roche Diagnostics). The protein concentration of each sample was determined using a BCA protein assay kit (QB PERBIO). The cell lysates were treated with DNase I (Takara), and then dissolved in sample buffer. The same amounts (approximately 25 μg) of cell lysates were subjected to SDS-PAGE. Following electrophoresis, proteins were transferred to a PVDF membrane and probed with anti-rat Foxp3 (FJK-16s; eBioscience) and anti-β-actin (AC40; Sigma) antibodies followed by secondary antibodies conjugated to horseradish peroxidase. Proteins were visualized by staining with ECL+ (GE healthcare) followed by evaluation with the LAS-1000 plus system (Fuji film) using Image Gauge Version 3.4 software (Fuji film).

2.3. Quantitative RT-PCR of mRNAs

Total RNA was extracted using the Absolutely RNA® Miniprep Kit (Stratagene) and treated with RNase-Free DNase I (Stratagene) to minimize contamination of chromosomal DNA. The RNA concentration was measured by absorbance at 260 nm, and purity was ascertained by the OD260/280 ratio.

The foxp3, HBZ and g3pdh mRNAs were quantified by real-time PCR using LightCycler PCR instrument (Roche Diagnostics). Quantitative RT-PCR of foxp3 and g3pdh was performed by LightCycler RNA amplification Kit Hybridization Probes (Roche Diagnostics) with the following primer pairs and hybridization probes: foxp3 forward primer 5′-CAG CAC CTT TCC AGA GTT CTT C -3′ and the reverse primer 5′- GCG TGT GAA CCA ATG GTA GAT T-3′, the hybridization probes 5′-CCC TTT CAC CTA TGC CAC CCT CAT CC- (FITC)-3′ and 5′- (LCRed640)- TGG GCC ATC CTG GAA GCT CCA GAG AGG-3′; g3pdh forward primer 5′-AAG GTC ATC CCA GAG CTG AA -3′ and the reverse primer 5′-ATG TAG GCC ATG AGG TCC AC-3′, the hybridization probes 5′-TCC CAT TCT TCC ACC TTT GAT TGC TGG G- (FITC)-3′ and 5′-(LCRed705)-TGG CAT TGC TCT CAA TGA CAA CTT TGT GAA GCT CA-3′. HBZ mRNA was quantified using LightCycler RNA amplification Kit SYBR Green 1 (Roche Diagnostics, Mannheim) with the following primer pairs: forward primer 5′-ATG GCG GCC TCA GGG CTG TTT CGA TGC TT-3′ and the reverse primer 5′-CTG CCG ATC ACG ATG CGT TT-3′. RNA (200 ng) was subjected to RT-PCR reaction according to the instruction manual. The optimum concentration of $MgCl_2$ was 7 mM for foxp3 and g3pdh, and 5 mM for HBZ amplification. 20 μl of a RT-PCR mixture in a capillary tube containing were subjected to RT-PCR reaction including incubation for 30 min at 55 °C and 30 s at 95 °C, and then 35 cycles of 5 s at 95 °C and 15 s at 60 °C and 9 s at 72 °C. The copy numbers of cDNA in the samples were estimated based on a standard regression curve using the LightCycler Software version 3 (Roche Diagnostics). The standard curve was obtained by amplifying 1×10^3 to 1×10^7 copies of the Foxp3 and G3PDH cDNA fragments with the corresponding pair of primers. The copy numbers of Foxp3 cDNA were normalized by dividing with those of the G3PDH cDNA in the same samples.

2.4. Analysis of cell surface markers

Expression of cell surface markers was examined by flow cytometry. Briefly, 1×10^6 of cells were stained with various mouse monoclonal antibodies for 30 min on ice, washed three

times with 1% BSA in PBS, and then stained with FITC-conjugated goat anti-mouse IgG + IgM antibody. After being washed, the cells were fixed with 1% formalin in PBS, prior to analysis by FACScalibur (Becton Dickinson). Antibodies to rat CD3, CD4, CD25, CD28 and major histocompatibility complex class 1 (MHC-1; RT1.A) were purchased from BD Pharmingen Co. Anti-rat CD5 and CTLA-4 (CD154) antibodies were from eBioscience Co.

2.5. Detection of TGF-β1 in culture supernatant

HTLV-1$^+$ cells (10^5/well) were cultured in 24-well flat-bottom plates for 4 days. The amount of TGF-β1 in the culture supernatant was quantified using TGF-β1 enzyme-linked immunosorbent assay (ELISA) (R&D Systems).

2.6. T cell proliferation analysis

To examine the ability of HTLV-1-infected rat cells to suppress the proliferation of T cells, F344 rat splenocytes (7.5×10^5 cells) were labeled with 10 μM CFSE solution (Invitrogen) according to the manufacture's manual, and stimulated by plate-coated anti-rat CD3 mAb (G4.18 eBioscience) and 0.5 μg/ml anti-rat CD28 mAb (JJ319 eBioscience) in 10 U/ml of IL-2 containing medium. Then, 5.0×10^5 of mitomycin C (50 μg/ml)-treated HTLV-1-infected rat cell lines were added in the culture. T cell proliferation was evaluated by calibrating the CFSE dilution with FACScalibur 3 days after commencing the co-culture.

3. Results

3.1. Foxp3 expression in HTLV-1-infected rat cell lines

To assess the expression of Foxp3 in rat HTLV-I-infected cell lines that we established previously, we performed Western blot analysis (Fig. 1) and RT-PCR (Fig. 2A). These analyses revealed that 10 of 22 cell lines expressed foxp3 mRNA and protein (Figs. 1, 2A and Table 1). Next, we compared the expression level of foxp3 mRNA among the cell lines. Quantitative RT-PCR analysis revealed that foxp3 mRNA expression level was variable in each cell line (Fig. 2B and Table 1), but parallel to protein level (Figs. 1 and 2B). Interestingly, we observed the enhanced expression of foxp3 mRNA in IL-2-dependent cell lines compared with their factor-independent counterparts that were cultured in the absence of IL-2 (Fig. 2B). To examine the effect of IL-2 on the Foxp3 expression, we cultured the IL-2-independent cell lines in the presence of IL-2 for 3 weeks and compared the Foxp3 expression levels. As shown in Fig. 2C, Foxp3 expression was not restored in the presence of IL-2.

Next, we addressed whether the expression of Foxp3 is associated with HBZ (HTLV-1 bZIP factor) that is a nuclear protein encoded with minus strand RNA of HTLV-1. HBZ is detected in majority of ATL cells whereas Tax expression is often repressed or lacked [21]. As the case of ATL cells, the HBZ mRNA was detected in all of the subjected rat HTLV-1$^+$ cell lines albeit with a great variability in the expression level of each cell line (Fig. 2D and Table 1). However, there were no association between HBZ and foxp3 mRNA expression (Fig. 2E).

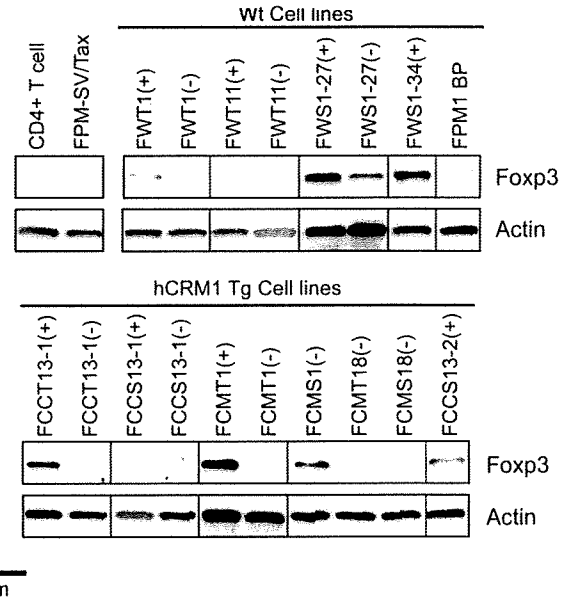

Fig. 1. Foxp3 expression in established rat HTLV-1 transformed cell lines. Western blot analysis shows the relative levels of Foxp3 in each cell line. Splenic CD4$^+$ T cell extract was used as positive control, epithelial cell line FPM-SV/Tax derived from F344 background rat used as negative control. Each protein level was determined on western blots containing 25 μg of total protein per lane.

3.2. Characterization of Foxp3 expressing cell lines

To characterize the rat Foxp3 positive cell lines in more detail, we examined the production of TGF-β1 and surface markers of the established cell lines. The TGF-β1 concentration of culture medium could be detected from 2 of Foxp3 positive and 2 of Foxp3 negative cell lines (Fig. 3A). These data indicate that there are no correlation between TGF-β1 secretion and Foxp3 expression. As shown in Fig. 3B, all subjected cell lines were CD25 and MHC class 1 positive, whereas CD4 and CD3 expression patterns were variable among the cell lines. Only 2 cell lines exhibited CD4$^+$ CD25$^+$ phenotypes like regulatory T cell, whereas other 4 cell lines did not express surface CD4. We also examined the expression of CD5 and found that 8 of 10 Foxp3 positive cell lines expressed surface CD5 (Fig. 4A), suggesting significant correlation between surface CD5 and Foxp3 expression (Fig. 4B).

CTLA-4 (CD154) is known as one of the regulatory T cell markers controlled by Foxp3 and suggested its relation to Treg suppressive function [4,7]. So we addressed the relation of CTLA-4 to Foxp3 expression in HTLV-1-infected rat cell lines. As shown in Fig. 4C, 10 of 19 cell lines exhibited weak CTLA-4 expression. However we did not found the enhanced expression of CTLA-4 in Foxp3 positive cell lines.

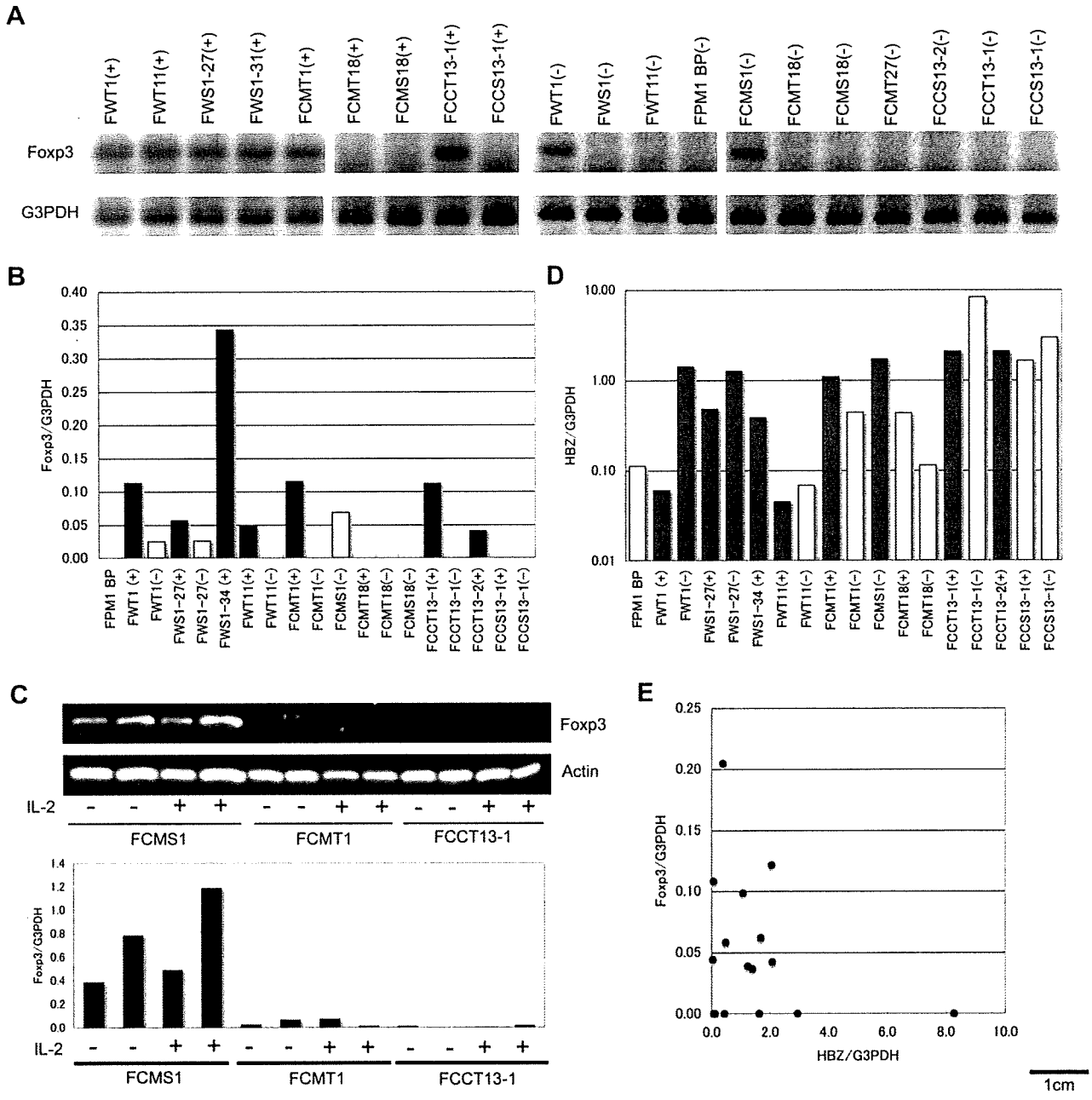

Fig. 2. Foxp3 and HBZ mRNA expression in established cell lines. (A) Detection of the foxp3 mRNA in cell lines by RT-PCR. RNA extracted from each cell line was subjected to RT-PCR with primers for Foxp3 and with primers for G3PDH as an internal control. (B) The expression level of foxp3 mRNA was measured by quantitative real-time RT-PCR. The copy number of synthesized Foxp3 cDNA was normalized by dividing with the copy number of synthesized G3PDH cDNA in the same sample. Black and grey bar indicate IL-2 dependent and independent cell lines, respectively. (C) Foxp3 protein (upper panel) and mRNA (lower panel) expression of IL-2 independent cell lines that cultured with (+) or without (-) IL-2 (10 U/ml) for 3 weeks. (D) The expression level of HBZ mRNA was measured by real-time RT-PCR. The copy number of synthesized HBZ cDNA was normalized by dividing with the copy number of synthesized G3PDH cDNA in the same sample. Black and white bar indicate Foxp3 positive and negative cell lines, respectively. The negative control did not show any signals. (E) Correlation between the relative expression of Foxp3 and HBZ mRNAs in the subjected 18 cell lines.

3.3. The immunosuppressive activity of Foxp3 positive cell lines

Next, we examined whether Foxp3 and/or CTLA4 expressing HTLV-1-infected rat T cell lines suppress the proliferation of naïve T cells. To assess the suppressive function, rat T cell lines were co-cultured with CFSE-labeled naïve T cells that were stimulated by anti-CD3 monoclonal antibody (mAb). Suppressive effects of HTLV-1-infected cell lines were evaluated by CFSE dilution in the naïve T cells. As shown in Fig. 5, proliferation of naïve T cells was significantly suppressed by 4 of 6 Foxp3 positive cell lines and 2 of 6 cell

Table 1
Established cell lines and Foxp3 or HBZ expression.

Cell line	Dependent of independent[a]	Presence of abcence of[b]	Detected or not[c]		Relative mRNA expression values to G3PDH	
			Foxp3 Detection method:			
	IL−2dependency	hCRM1	Western blot	RT−PCR	Foxp3	HBZ
FWT1(+)	+	−	+	+	0.112	0.060
FWT1(−)	−	−	−	+	0.024	1.394
FWT11(+)	+	−	+	+	0.047	0.045
FWT11(−)	−	−	−	−	0.000	0.068
FWS1(−)	−	−	N.S	−	N.S	N.S
FWS1−27(+)	+	−	+	+	0.056	0.475
FWS1−27(−)	−	−	+	N.S	0.026	1.239
FWS1−34(+)	+	−	+	N.S	0.342	0.382
FPM1 BP	−	−	−	−	0.000	0.112
FCMT1(+)	+	+	+	+	0.115	1.078
FCMT1(−)	−	+	−	N.S	0.000	0.436
FCMS1(−)	−	+	+	+	0.068	1.688
FCMT18(+)	+	+	−	−	0.000	0.429
FCMT18(−)	−	+	−	−	0.000	0.113
FCMS18(−)	−	+	−	−	0.000	N.S
FCMT27(−)	−	+	N.S	−	N.S	N.S
FCCT13−1(+)	+	+	+	+	0.111	2.056
FCCT13−1(−)	−	+	−	−	0.000	8.260
FCCT13−2(+)	+	+	+	N.S	0.040	2.076
FCCS13−1(+)	+	+	−	−	0.000	1.630
FCCS13−1(−)	−	+	−	−	0.000	2.943
FCCS13−2(−)	−	+	N.S	−	N.S	N.S

[a] +, IL-2 dependent stage; -, IL-2 independent stage.
[b] +, Positive; −, Negative.
[c] +, Detected; -, Not detected; N.S, Not subjected.

lines that were Foxp3 negative but express CTLA-4, Treg associated molecule (Fig. 4C). Notably, all 3 Foxp3$^+$ CTLA-4$^+$ cell lines showed the suppressive activity (Figs. 4C and 5). These results demonstrate that some HTLV-1-infected rat cell lines have suppressive function as the case of human ATL cells, and suggest that Foxp3 and CTLA-4 may be involved in the suppression.

4. Discussion

Some ATL cells have been reported to express higher level of Foxp3 and exhibited Treg cell like activity [11,14]. Here we show that some Foxp3 positive HTLV-1-infected rat cell lines, like Treg cells, suppress TCR-stimulated naïve T cell division (Fig. 5). This suppressive function may be dependent on cell-to-cell contact, because the culture medium of suppressive cell lines didn't affect the T cell division (data not shown), consistent with the previous report that described contact dependent Treg like activity of ATL and HTLV-1-infected cells [14]. Therefore, our rat model is useful to examine a role of the suppressive activity of HTLV-1-infected cells in HTLV-1 infection and ATL development.

We found 3 of 4 Foxp3$^+$ suppressive cell lines expressed CTLA-4 (Fig. 4C). Moreover, we identified two suppressive cell lines expressing CTLA-4 but not Foxp3 (Figs. 4C and 5), suggesting the association of cellular CTLA-4 expression with suppressive function. Although CTLA-4 contribution to Treg cell function is controversial because Foxp3$^+$ Treg cells differentiated in CTLA-4 KO mice suppress naïve T cell proliferation [5], it has been recently demonstrated that Treg cells derived from CTLA-4 conditional KO mice show impaired suppressive function [7]. Furthermore, the suppression mechanism has been reported to be mediated by CTLA-4 inducing down-regulation of CD80 and CD86 on antigen presenting cells (APC) [7]. However, in our experiments co-stimulatory signal for naïve T cells was mediated by anti-CD28 mAb but not by APC (Fig. 5). Thus, it is possible that CTLA-4 affected CD80 and CD86 on stimulated T cells directly to suppress their proliferations. This notion is consistent with facts that the expression of CD80 and CD86 is induced by activation of human and mouse T cells and that T cells from CD80/CD86-deficient mice are resistant to suppression by Tregs [6,22]. Further experiments should reveal the role of CTLA-4 in Treg cell like function of HTLV-1-infected rat cells more clearly.

It has been reported that CTLA-4 expression is normally induced by T cell activation [6] or exogenous Foxp3 gene transduction [3]. In ATL cells, there is positive correlation between foxp3 mRNA expression levels and percentages of CTLA-4 positive leukemic cells [12]. On contrary, we found some CTLA-4$^-$ Foxp3$^+$ and CTLA-4$^+$ Foxp3$^-$ cell lines (Fig. 4C and D), suggesting that the Foxp3 expression is not enough to induce CTLA-4 expression and that Foxp3-independnt CTLA-4 induction pathway(s) may be present in some HTLV-1-infected rat cell lines.

Several pathways for induction of Foxp3 has been identified in human and mouse Treg cells [23]. Particularly, IL-2 and TGF-β has been reported as the crucial factors [23]. When we

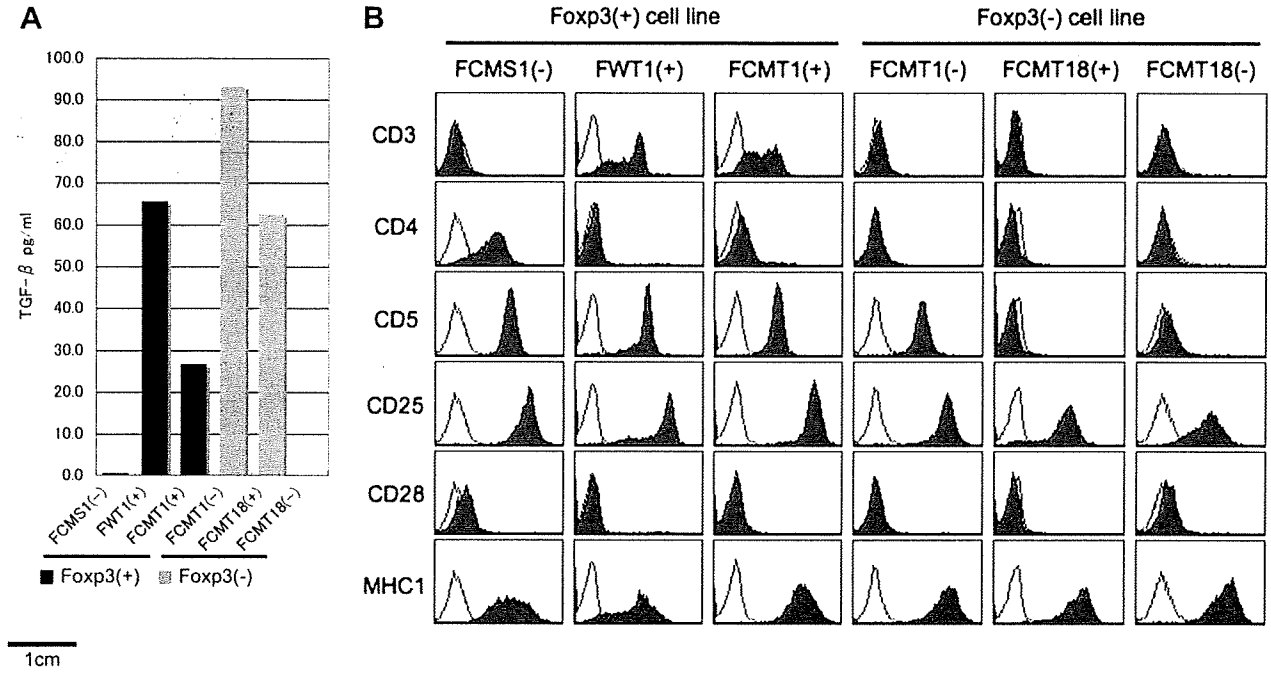

Fig. 3. TGF-β1 and surface marker analyses of Foxp3 positive or negative cell lines. (A) TGF-β1 levels in the supernatant of 4-day cultures were quantified by ELISA. (B) The expression of surface antigen CD3, CD4, CD5, CD25, CD28 and MHC1 was analyzed by flow cytometry. Solid histograms show the cells stained with each marker specific monoclonal antibody, and open histograms show the cells stained with control mouse IgG.

measured the concentration of TGF-β in the culture medium of the HTLV-1-infected rat cell lines, we did not find any correlation between expressions of TGF-β and Foxp3 (Fig. 3A), indicating less contribution of TGF-β to Foxp3 expression in our rat model system. On the other hand, Foxp3 expression was higher in the IL-2 dependent HTLV-1$^+$ rat cell lines and then decreased or completely disappeared in the IL-2 independent cells (Figs. 1 and 2B), suggesting a substantial role of IL-2 in maintaining the expression of Foxp3 in the HTLV-1-transformed rat cell lines. It is consistent with the report describing that IL-2 promotes Foxp3 expression in human Treg cells [24]. It has been also demonstrated that the induction of Foxp3 expression is dependent on STAT3/STAT5-associated signal transduction pathway [24]. Moreover, STAT5 has been reported to be activated in the HTLV-1-transformed human cells [25]. Taken together, we propose that IL-2 induces the Foxp3 via STAT dependent way in the HTLV-1-infected cell, especially at the IL-2 dependent stage during the cellular transformation. However, there were some IL-2 dependent HTLV-1-infected cell lines that do not express Foxp3 (Figs. 1, 2A and B), suggesting the requirement of other factor(s) for the induction of Foxp3.

CD5 is known as a T cell marker and the negative regulator of TCR-mediated signal transduction [26]. Sakaguchi et al. demonstrated that depletion of the CD5^{high} T cell population also depleted majority of CD4$^+$ CD25$^+$ T cells simultaneously [27]. Recently, the inhibitory role of CD5 has been reported in the murine T reg cell suppressive function [28]. In our data, CD5 expression was significantly correlated with Foxp3 expression in HTLV-1-infected cells (Fig. 4A, B). One of CD5$^-$ Foxp3$^+$ cell line FWS1-27(-) exhibited suppressive function but not in another cell line FCCT13-1(+). Moreover, a CD5$^+$ Foxp3$^-$ cell line FWT1(+) could not suppress the naïve T cell proliferations (Fig. 5). Taken together, the results suggest that there is no apparent association between CD5 expression and Treg cell like suppressive function in our system.

Previous reports identified some Foxp3$^+$ ATL cells that could not suppress the proliferation of T cells [14]. Similarly, in our rat system there are some Foxp3 positive cell lines, which lack the immunosuppressive function (Fig. 5). These results indicate that Foxp3 may be essential but not sufficient for the T reg like suppressive activity of HTLV-1-infected cell lines. Recent studies have demonstrated transcription factors, NF-AT [29] and AML1/Runx1 [30], are involved in the induction of suppressive function of Treg cells in concert with Foxp3. These factors may also associate with Treg cell like function of the HTLV-1-infected cell lines. Both types of Foxp3 expressing HTLV-1-infected cell lines that do and do not suppress proliferation of naïve T cells (Fig. 5) may serve for advanced experiments that are focused on NF-AT and/or AML1/Runx1 to reveal the relationships of Foxp3-associated intracellular molecules to Treg cell like functions of HTLV-1-infected cell lines and ATL cells.

There are several reports that suggest relation of Foxp3 expression to ATL progression [13]. Namely, ATL cells or HTLV-1-infected cells that acquire Treg cell like function invoked by Foxp3 may impair the cellular immune reactions to cause exacerbation of HTLV-1-associated diseases. However, there were no useful models to analyze the association of

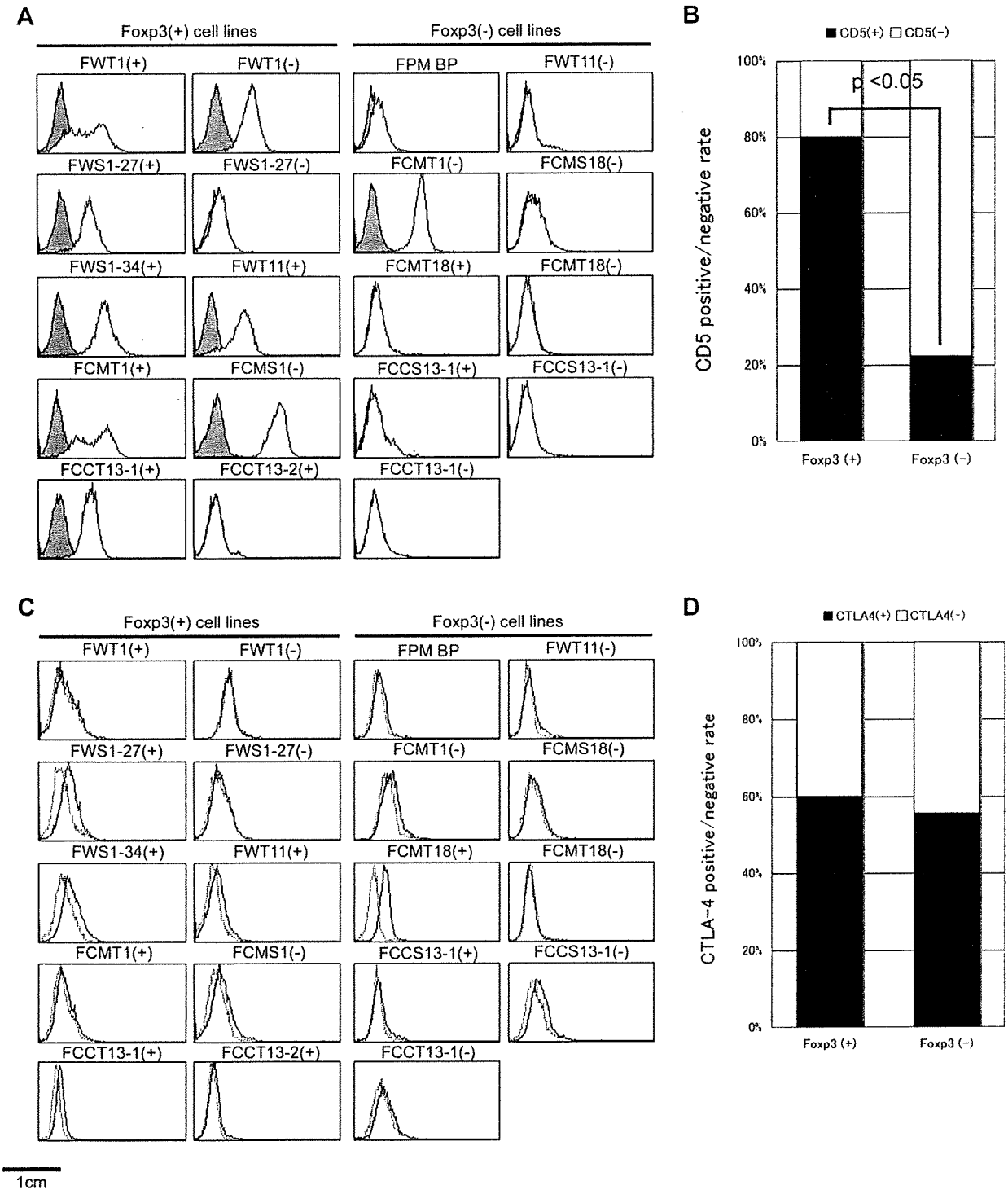

Fig. 4. Surface CD5 and CTLA-4 expression of Foxp3 positive or negative cell lines. The expression of surface CD5 (A) and CTLA4 (C) was analyzed by flow cytometry. (A) Cells were stained with anti-rat CD5 (grey) or control (black) antibodies. (C) Cells were stained with the rat CTLA4 (grey) or control (open) mouse IgG. The positive rate of CD5 (B), or CTLA4 (D) expression in Foxp3 positive or negative cell line group. Black area indicates positive rate in each group, and white area indicates CD5 negative rate. The statistical significance of differences was determined by chi square test.

Foxp3 expressing HTLV-1-infected cells with ATL or related immunodeficiency *in vivo*. Here we identified four HTLV-1-infected cell lines with Foxp3 expression, which have immunosuppressive function. Furthermore, we found three Foxp3$^+$ CTLA-4$^+$ and two Foxp3$^-$ CTLA-4$^+$ cell lines that suppress proliferation of naïve T cells. Our data suggest that the cells expressing Treg cell-associated factors such as Foxp3 and CTLA4 are involved in the suppressive functions. Since rat

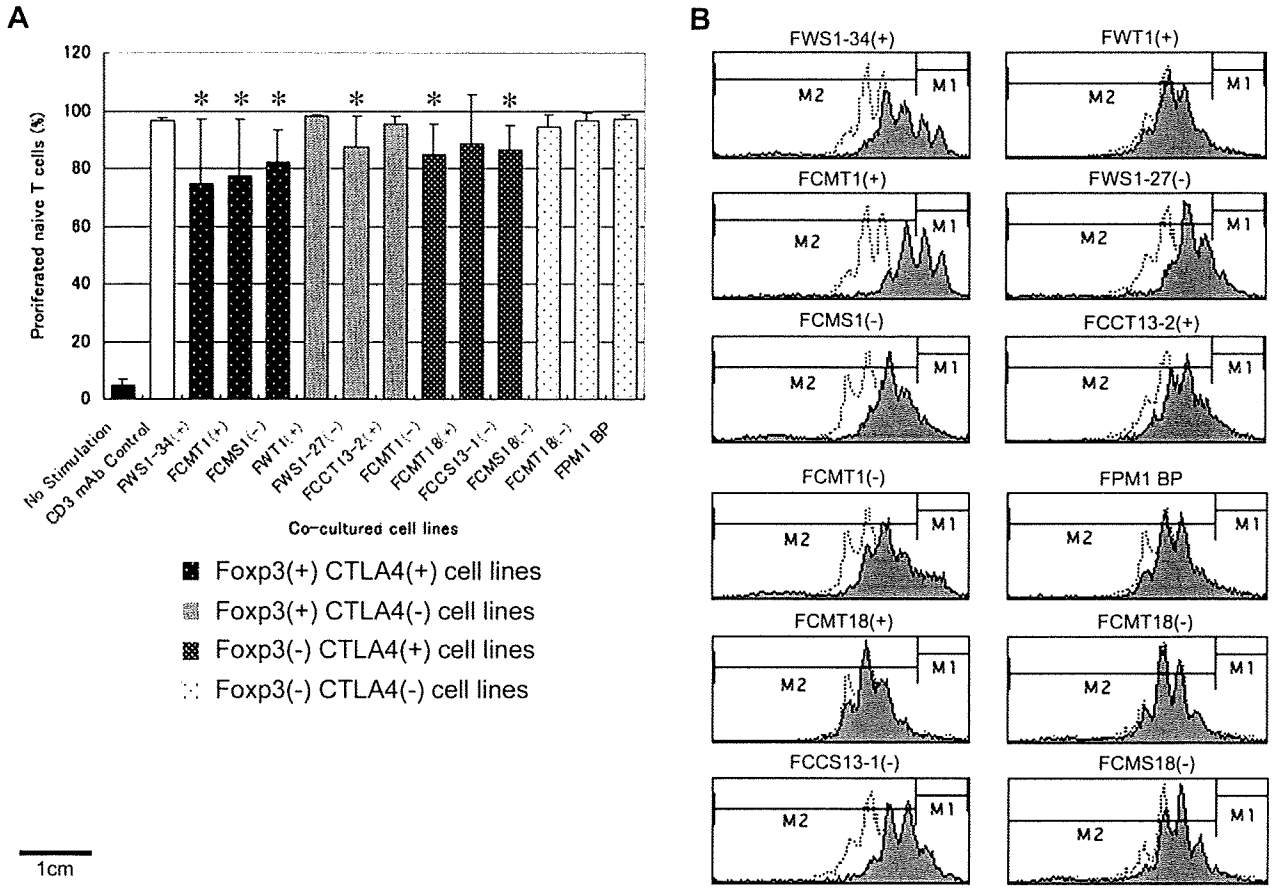

Fig. 5. Suppressive function of Foxp3 and/or CTLA-4 expressing HTLV-1-infected cell lines to stimulated naïve T cells. (A) Suppressive activity of HTLV-1-infected rat cell lines was estimated based on the percentage of proliferated CFSE-labeled T cells. (*) indicates the $p < 0.05$ compared with CD3 mAb control. (B) Profiles of proliferated CFSE-labeled T cells after co-culture with indicated cell lines (dark histograms) and CD3 mAb control (thin histograms) are presented. M1 region was gated for non-divided T cells estimated with non-stimulated control and M2 region was gated for proliferated cells.

model allows *in vivo* experiments, the present results may provide the basis for further studies on the relationships of Foxp3 with HTLV-1-associated pathogenesis.

Acknowledgments

We thank A. Hirano and N. Mizuno for excellent technical assistance. This study was supported by grants from the Ministry of Education, Culture, Sports, Science and Technology (Japan) and the Ministry of Health, Labour and Welfare (Japan) and the Japan Society for the Promotion of Science (Japan).

References

[1] M. Miyara, S. Sakaguchi, Natural regulatory T cells: mechanisms of suppression, Trends Mol. Med. 13 (2007) 108–116.
[2] X. Cao, S.F. Cai, T.A. Fehniger, J. Song, L.I. Collins, D.R. Piwnica-Worms, T.J. Ley, Granzyme B and perforin are important for regulatory T cell-mediated suppression of tumor clearance, Immunity 27 (2007) 635–646.
[3] S. Hori, T. Nomura, S. Sakaguchi, Control of regulatory T cell development by the transcription factor Foxp3, Science 299 (2003) 1057–1061.
[4] T. Takahashi, T. Tagami, S. Yamazaki, T. Uede, J. Shimizu, N. Sakaguchi, T.W. Mak, S. Sakaguchi, Immunologic self-tolerance maintained by CD25(+)CD4(+) regulatory T cells constitutively expressing cytotoxic T lymphocyte-associated antigen 4, J. Exp. Med. 192 (2000) 303–310.
[5] Q. Tang, E.K. Boden, K.J. Henriksen, H. Bour-Jordan, M. Bi, J.A. Bluestone, Distinct roles of CTLA-4 and TGF-beta in CD4 + CD25+ regulatory T cell function, Eur. J. Immunol. 34 (2004) 2996–3005.
[6] D.M. Sansom, L.S. Walker, The role of CD28 and cytotoxic T-lymphocyte antigen-4 (CTLA-4) in regulatory T-cell biology, Immunol. Rev. 212 (2006) 131–148.
[7] K. Wing, Y. Onishi, P. Prieto-Martin, T. Yamaguchi, M. Miyara, Z. Fehervari, T. Nomura, S. Sakaguchi, CTLA-4 control over Foxp3+ regulatory T cell function, Science 322 (2008) 271–275.
[8] T. Uchiyama, Human T cell leukemia virus type I (HTLV-I) and human diseases, Annu. Rev. Immunol. 15 (1997) 15–37.
[9] M. Matsuoka, Human T-cell leukemia virus type I and adult T-cell leukemia, Oncogene 22 (2003) 5131–5140.
[10] K. Karube, K. Ohshima, T. Tsuchiya, T. Yamaguchi, R. Kawano, J. Suzumiya, A. Utsunomiya, M. Harada, M. Kikuchi, Expression of FoxP3, a key molecule in CD4CD25 regulatory T cells, in adult T-cell leukaemia/lymphoma cells, Br. J. Haematol. 126 (2004) 81–84.
[11] T. Kohno, Y. Yamada, N. Akamatsu, S. Kamihira, Y. Imaizumi, M. Tomonaga, T. Matsuyama, Possible origin of adult T-cell leukemia/lymphoma cells from human T lymphotropic virus type-1-infected regulatory T cells, Cancer Sci. 96 (2005) 527–533.
[12] Y. Matsubara, T. Hori, R. Morita, S. Sakaguchi, T. Uchiyama, Phenotypic and functional relationship between adult T-cell leukemia cells and regulatory T cells, Leukemia 19 (2005) 482–483.

[13] G. Roncador, J.F. Garcia, L. Maestre, E. Lucas, J. Menarguez, K. Ohshima, S. Nakamura, A.H. Banham, M.A. Piris, FOXP3, a selective marker for a subset of adult T-cell leukaemia/lymphoma, Leukemia 19 (2005) 2247–2253.

[14] S. Chen, N. Ishii, S. Ine, S. Ikeda, T. Fujimura, L.C. Ndhlovu, P. Soroosh, K. Tada, H. Harigae, J. Kameoka, N. Kasai, T. Sasaki, K. Sugamura, Regulatory T cell-like activity of Foxp3+ adult T cell leukemia cells, Int. Immunol. 18 (2006) 269–277.

[15] T. Ohashi, S. Hanabuchi, H. Kato, Y. Koya, F. Takemura, K. Hirokawa, T. Yoshiki, Y. Tanaka, M. Fujii, M. Kannagi, Induction of adult T-cell leukemia-like lymphoproliferative disease and its inhibition by adoptive immunotherapy in T-cell-deficient nude rats inoculated with syngeneic human T-cell leukemia virus type 1-immortalized cells, J. Virol. 73 (1999) 6031–6040.

[16] M. Nomura, T. Ohashi, K. Nishikawa, H. Nishitsuji, K. Kurihara, A. Hasegawa, R.A. Furuta, J. Fujisawa, Y. Tanaka, S. Hanabuchi, N. Harashima, T. Masuda, M. Kannagi, Repression of tax expression is associated both with resistance of human T-cell leukemia virus type 1-infected T cells to killing by tax-specific cytotoxic T lymphocytes and with impaired tumorigenicity in a rat model, J. Virol. 78 (2004) 3827–3836.

[17] Y. Hakata, M. Yamada, H. Shida, A multifunctional domain in human CRM1 (exportin 1) mediates RanBP3 binding and multimerization of human T-cell leukemia virus type 1 Rex protein, Mol. Cell. Biol. 23 (2003) 8751–8761.

[18] Y. Hakata, M. Yamada, H. Shida, Rat CRM1 is responsible for the poor activity of human T-cell leukemia virus type 1 Rex protein in rat cells, J. Virol. 75 (2001) 11515–11525.

[19] X. Zhang, Y. Hakata, Y. Tanaka, H. Shida, CRM1, an RNA transporter, is a major species-specific restriction factor of human T cell leukemia virus type 1 (HTLV-1) in rat cells, Microbes Infect. 8 (2006) 851–859.

[20] R. Takayanagi, T. Ohashi, E. Yamashita, Y. Kurosaki, K. Tanaka, Y. Hakata, Y. Komoda, S. Ikeda, Y. Tsunetsugu-Yokota, Y. Tanaka, H. Shida, Enhanced replication of human T-cell leukemia virus type 1 in T cells from transgenic rats expressing human CRM1 that is regulated in a natural manner, J. Virol. 81 (2007) 5908–5918.

[21] Y. Satou, J. Yasunaga, M. Yoshida, M. Matsuoka, HTLV-I basic leucine zipper factor gene mRNA supports proliferation of adult T cell leukemia cells, Proc. Natl. Acad. Sci. U.S.A. 103 (2006) 720–725.

[22] S. Paust, L. Lu, N. McCarty, H. Cantor, Engagement of B7 on effector T cells by regulatory T cells prevents autoimmune disease, Proc. Natl. Acad. Sci. U.S.A. 101 (2004) 10398–10403.

[23] L. Zhang, Y. Zhao, The regulation of Foxp3 expression in regulatory CD4(+)CD25(+)T cells: multiple pathways on the road, J. Cell. Physiol. 211 (2007) 590–597.

[24] E. Zorn, E.A. Nelson, M. Mohseni, F. Porcheray, H. Kim, D. Litsa, R. Bellucci, E. Raderschall, C. Canning, R.J. Soiffer, D.A. Frank, J. Ritz, IL-2 regulates FOXP3 expression in human CD4 + CD25+ regulatory T cells through a STAT-dependent mechanism and induces the expansion of these cells in vivo, Blood 108 (2006) 1571–1579.

[25] T.S. Migone, J.X. Lin, A. Cereseto, J.C. Mulloy, J.J. O'Shea, G. Franchini, W.J. Leonard, Constitutively activated Jak-STAT pathway in T cells transformed with HTLV-I, Science 269 (1995) 79–81.

[26] J.J. Perez-Villar, G.S. Whitney, M.A. Bowen, D.H. Hewgill, A.A. Aruffo, S.B. Kanner, CD5 negatively regulates the T-cell antigen receptor signal transduction pathway: involvement of SH2-containing phosphotyrosine phosphatase SHP-1, Mol. Cell. Biol. 19 (1999) 2903–2912.

[27] S. Sakaguchi, N. Sakaguchi, M. Asano, M. Itoh, M. Toda, Immunologic self-tolerance maintained by activated T cells expressing IL-2 receptor alpha-chains (CD25). Breakdown of a single mechanism of self-tolerance causes various autoimmune diseases, J. Immunol. 155 (1995) 1151–1164.

[28] T. Dasu, J.E. Qualls, H. Tuna, C. Raman, D.A. Cohen, S. Bondada, CD5 plays an inhibitory role in the suppressive function of murine CD4(+) CD25(+) T(reg) cells, Immunol. Lett. 119 (2008) 103–113.

[29] Y. Wu, M. Borde, V. Heissmeyer, M. Feuerer, A.D. Lapan, J.C. Stroud, D.L. Bates, L. Guo, A. Han, S.F. Ziegler, D. Mathis, C. Benoist, L. Chen, A. Rao, FOXP3 controls regulatory T cell function through cooperation with NFAT, Cell 126 (2006) 375–387.

[30] M. Ono, H. Yaguchi, N. Ohkura, I. Kitabayashi, Y. Nagamura, T. Nomura, Y. Miyachi, T. Tsukada, S. Sakaguchi, Foxp3 controls regulatory T-cell function by interacting with AML1/Runx1, Nature 446 (2007) 685–689.